PROJECT OFFSHORE DEEP SLOPES, PHASE I

APPENDIX

FINAL REPORT

Prepared for:

Chevron Canada Resources
Pan Canadian
Murphy Oil
ExxonMobil
Minerals Management Services
Norsk Hydro, Statoil

Prepared by:

C-CORE, OTRC, GSC, NGI

C-CORE Report:

01-C12

April 2002

C-CORE
Captain Robert A. Bartlett Building
Morrissey Road
St. John's, NF
Canada A1B 3X5

T: (709) 737-8354
F: (709) 737-4706

Info@c-core.ca
Www.c-core.ca

The correct citation for this report is:

C-CORE (2002). Project Offshore Deep Slopes – Phase I (Appendix). Final Report. Prepared for: Chevron Canada Resources, Pan Canadian, Murphy Oil, ExxonMobil, Minerals Management Services, Norsk Hydro and Statoil. Prepared by: C-CORE, OTRC, GSC and NGI. C-CORE Publication 01-C12.

Project Team:

Lars Andersen (NGI)
Jack Clark (C-CORE)
Wayne Dunlap (OTRC)
Peijun Guo (C-CORE)
Richard Hanke (C-CORE)
Jocolyn Grozic (University of Calgary)
Ryan Phillips (C-CORE)
Dick Pickrill (GSC)
David Piper (GSC)
Gary Sonnichsen (GSC)
Abigail Steel (C-CORE)
Skip Ward (OTRC)
Stephen Wright (University of Texas)

TABLE OF CONTENTS

LIST OF FIGURES

LIST OF TABLES

APPENDIX 1: ADDITIONAL INFORMATION ON THE CASE STUDIES

Kitimat Submarine Slide

1.1 Location of Slide and age of failure:
This slide is located in the Kitimat Inlet of the Douglas Channel system (53°59' N 128° 41' W), British. The failure in question occurred at 10:05 a.m., on April 27, 1975 (Murty & Brown, 1979). The slide occurred approximately 53 minutes after the occurrence of low tide, and generated two, possibly three large waves, the largest estimated to be 8.2 m crest to trough (Murty & Brown, 1979). On October 17, 1974, a wave 2.4 m in height was observed at 11:05 a.m., shortly after low tide. It was believed that the wave was caused by a submarine slide, however evidence is only circumstantial (Johns et al., 1986). Several other events are also believed to have occurred in the area between 1952 and 1968, and also in 1971 (Johns et al., 1986). In all instability events failure began in the delta front/sidewall area of the fjord (Johns et al., 1986).

1.2 Detailed Bathymetry of site:
Figure A1.2 Kitimat Arm three dimensional slide morphology (Prior et al., 1982).

1.3 Type of slide and type(s) of soil failure (slide, slump, mass flow, turbidity current, etc.):
The failure at Kitimat seems to have occurred through liquefaction. The soil failure was slumping and is attributed to shear failure in the soft marine clay (Campbell & Skermer, 1975; Murty & Brown, 1979).

1.4 Failure Mechanisms:
There were no major seismic activities or meteorological events reported at the time of the Kitimat slide (Murty & Brown, 1979). Some possible mechanisms that may have triggered the failure include: extreme low tides resulting in excessive pore water pressure within the clay and saturated soil conditions due to the melting snow from higher elevations and spring run-offs (Campbell & Skermer, 1975; Murty & Brown, 1979).

1.5 Geometry of Slide:

1.5.1 Amount of soil involved:
There was an estimated 60 x 10 m of material involved in the submarine slide according to Golder Associates (1975, *In*: Prior et al., 1982). Casagrande (1977) predicted the quantity of material involved was of the order of 10 m, while (Murty & Brown, 1979) estimated the upper limit for the total amount of soil involved in the slide to be about 26 x 10 m.

1.5.2 Depth of slide:
The slide depth had an average thickness of 7.5 m, with a maximum thickness of approximately 30 m (Golder Associates, 1975 *In*: Prior et. al., 1982).

1.5.3 Slope angle:
According to Prior et al. (1982), the Kitimat slide area is composed of three different segments. A relatively short, steep head slope ranging between 4° and 7° on the delta front, an intermediate blocky zone with slopes averaging from 1° to 2°, and a large area more than 3.2 km long with slopes less than 1°. The 1975 slide involved the delta front

(slopes of 4° to 7°) and the western fjord wall, which has a gradient of up to 10° (Prior et. al., 1982).

1.5.4 Run out Distance:
The runout distance extends approximately 5 km (Prior et. al., 1982).

1.5.5 Water Depth:
The Kitimat Arm has an average water depth of 200 m (Prior et. al., 1982).

1.6 Slide Sediment Lithology:
The sediments involved in the slope failure were gravels, sands, silts and marine clays that were situated near the lower delta front (Prior et al., 1982). Sediments contained a high percentage of silt, ranging from silty sands on the delta front to clayey silts in deeper waters (Johns et al., 1986).

1.7 Degree of Consolidation:
Sediments were shown to be overconsolidated, with the overconsolidation ratio (OCR) decreasing with increasing depth of the material. This highly overconsolidated state is most likely the result of sediment proximity to the surface, where effective overburden pressures are low (Johns et al., 1986).

1.8 Sediment Accumulation Rate:
Based on Pb 210 measurements, soil accumulates from the Kitimat River at a rate of 2 to 5 mm/yr (Prior et al., 1982).

1.9 Subsurface stratigraphy to depth of slide plus 50% at the site adjacent to slide area (to predict pre-slide conditions):
The general Kitimat area is composed of transparent gray marine muds and sandy muds that were deposited and subsequently overlain by finely stratified muds and muddy sands with thin (1 – 2 m) sandy layers (Prior et al., 1982).

1.10 Geotechnical Properties of slide sediments and surrounding stable material:

1.10.1 Shear Strength: The following ranges for undrained shear strength were read from the graphs in Johns et al., 1986.
Delta Front: 11 – 35 kPa
Undisturbed Basin Floor: 7 – 17 kPa
Distal Debris Flow: 11 – 21 kPa

1.10.2 Water Content: The following ranges for water content were read from the graphs in Johns et al., 1986.
Delta Front: 44 – 60%

Undisturbed Basin Floor: 71 – 98%
Distal Debris Flow: 56 – 80%

1.10.3 Grain Density: 2.66 – 2.75 Mg/m (Johns et al., 1986).
Wet Bulk Density: 1.52 – 1.91 Mg/m (Johns et al., 1986).

1.10.4 Plasticity Index:
Kitimat sediments can be classified as inorganic silts and fine sands to clayey silts with low to medium plasticity. From the graphs in Johns et al., 1986, the plasticity index for the sediments range from 5% – 25%. Sediments with the lowest plasticity index and

liquid limit are found closest to the delta front whereas higher values are found in sediments located in the deeper fjord basin.

1.10.5 Other Properties:

The angles of shearing resistance for effective stress and corresponding effective cohesion values were 35.1° and 6.2 kPa for core 3 and 43.5° and 0 kPa for core 4 (Johns et al., 1986).

1.11 Possible releasing agents:

In April 1975, construction of a rock fill and dredged sand breakwater was initiated using material that was excavated from the bottom within and slightly seaward of the tidal zone. The construction in this area was still ongoing at the time of the slide. Slope failure is believed to have begun at the sidewall, in the vicinity of the breakwater (Johns et al., 1986).

1.12 Nature of constant loads on the soils:

In January of 1975, placement of 6 – 7.5 m of rock fill was placed in Moon Bay and in April 1975, a breakwater was constructed from rock fill and dredged material (Johns et al., 1986).

1.13 Nature of variable loads on the soils:

The day of the slide there was an extremely large tide, one of the largest that year, which ranged from 0.18 m to 6.2 m. The failure occurred approximately 53 minutes after low tide (Johns et al., 1986).

1.14 Evidence of tsunami generation:

There were at least two waves (possibly three) generated by the submarine slide in Kitimat inlet (Murty & Brown, 1979). The largest wave was estimated to be 8.2 m high, with a 4.6 m crest and 3.6 m trough (Murty & Brown, 1979).

1.15 Source type and quality of data:

Data was acquired using several different types of equipment. A digital 100 kHz side scan sonar system in conjunction with traverses with high resolution 500 kHz devices were used to do an extensive survey of the fjord floor. Six submersible dives were completed over the area using the Pisces IV, allowing visual inspection of the site and shallow coring of sediments. Also 3.5 kHz sub-bottom profilers were used on lines 100 – 200 m apart to determine subsurface geological and bathymetric conditions (Johns et al., 1986).

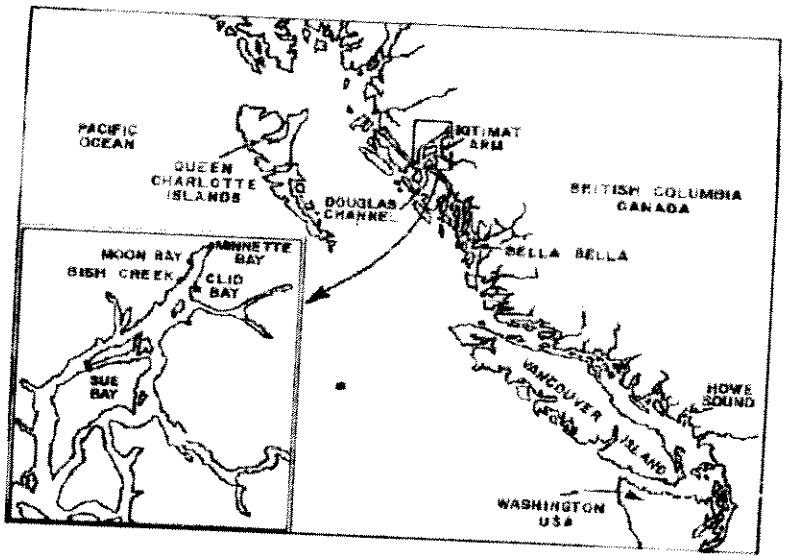

Figure A1.1: Location Map, Kitimat Arm. (Murty and Brown, 1979)

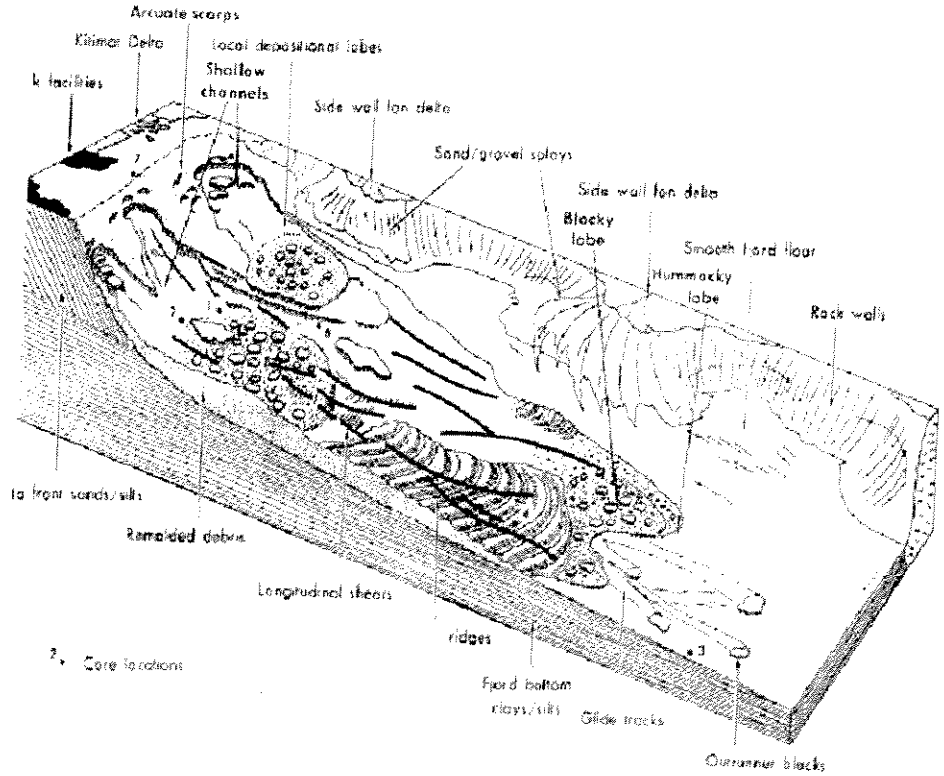

Figure A1.2: logical map of Kitimat Arm Failure (Murty and Brown, 1979).

References for Kitimat Arm Slide:

Campbell, D.B. and N.A. Skermer. (1975). Report to B.C. Water Resources Service on Investigation of Sea Wave at Kitimat, B.C. Golder Associates, Consulting Geotechnical Engineers, 224 West 8th Avenue, Vancouver, B.C. 9 pp., and diagrams.

Golder Associates, 1975, Report to British Columbia Water Resources Service on investigation of seawave at Kitimat, B.C.: Vancouver, Golder Associates, 9p.

Johns, M.W., Prior, D.B., Bornhold, B.D, Coleman, J.M. and Bryant, W.R., 1986. Geotechnical aspects of a submarine slope failure, Kitimat Fjord, British Columbia: Marine Geotechnology. v. 6; 3, Pages 243-279.

Murty, T.S. (1979) (In press). Submarine Slide-Generated Water Waves in Kitimat Inlet, B.C. J. of Phys. Res.

Murty, T.S. and Brown, R.E., 1979. The Submarine Slide of 27 April, 1975 in Kitimat Inlet and the Water Waves That Accompanied the Slide: Pacific Marine Science Report 79-11.

Prior, David B., Bornhold, Brian D., Coleman, James M., and Bryant, William R., 1982. Morphology of a submarine slide, Kitimat Arm, British Columbia. Geology 10(11).

Fraser River Delta Slide

2.1 Location of Slide and age of failure:
Figure A1.3 Fraser River Delta Location Map (Luternauer et al., 1994).

The Fraser River delta, just south of Vancouver, British Columbia, is the largest delta in western Canada. The Fraser River flows into the straight of Georgia on Canada's Pacific coast (Figure A1.3: Luternauer et al., 1994). The slide occurred in July of 1985 and resulted in the recession of the submarine sea valley to a point of 100 m from Sandy Heads lighthouse (Christian et al., 1994).

2.2 Detailed Bathymetry of site:
The Bathymetry of Fraser River Delta can be found in Luternauer et al. (1994).

2.3 Type of Slide/Types of soil failure (slide, slump, mass flow, turbidity currents, etc.):
The slide experienced at the mouth of the Fraser River in 1985 was due to liquefaction. This area has been recognized as having the highest liquefaction potential of any onshore sediment deposit (Christian et al., 1994).

2.4 Failure Mechanism:
Slope oversteeping due to high sedimentation rates found at the delta combined with tidal drawdown is thought to be a significant triggering mechanism for liquefaction flow slides (Christian et al., 1994). McKenna et al. (1992) theorized that the slide may have been due to a number of different events: rapid deposition of sediments, the presence of interstitial gas, strong tidal currents, cyclic wave loading and possibly earthquakes (*In:* Christian et al., 1997). However, a study conducted by Hungr (1993) demonstrated that the Fraser slide of 1985 was clearly unrelated to any historical seismic activities (*In:* Christian et al., 1997).

2.5 Geometry of Slide:

2.5.1 Amount of soil involved:
McKenna et al. (1992) estimated the amount of soil displaced during the Fraser slide to be at least 1 million meters (Christian et al., 1994). Luternauer et al. (1994) sited this value to be approximately 3 x 10 m.

2.5.2 Depth of slide:
The slide reached depths of up to 100 m (Christian et al., 1994).

2.5.3 Slope angles:
The slope angles of the Fraser Delta foreslope range in value from 0.5° to greater than 23°. The maximum slope angle found at the delta front does not exceed 15° (Christian et al., 1994). The western delta slope is inclined between 1° and 23°, but averages between 2° - 3°. The southern slope is ill-defined, but has a gentler gradient than that of the western slope (Luternauer et al., 1994).

2.5.4 Runout Distance:
The slides at the Fraser River delta appear to be self limiting as they have a tendency to stop when they reach the denser soil located at about 300 m from the canyon area (Hungr, 1993; Christian et al., 1997).

2.5.5 Water Depth:
The water depth is between 100 and 300 m (Christian et al., 1997)

2.6 Slide sediment lithology:

Sediments of the Fraser River delta are mainly Holocene in age (Christian et al., 1997). The sediments consist of interbedded silty sands and clayey silts (Christian et al., 1994). Delta slope sediments range from fine- grained sand to mud (Hart et al., 1992; Luternauer et al., 1994). The coarsest sediments occur on the upper slope near the mouth of the distributary channels and over most of the southern slope of Main Channel. West and North of the mouth of Main Channel, delta slope sediments gradually fine, from very fine-grained sand to very fine-grained sandy mud or mud (Luternauer et al., 1994).

2.7 Degree of Consolidation:
Most of the area south of the North Arm of the Fraser River and west of New Westminster is composed of unconsolidated sediments (Hamilton & Ricketts, 1994).

2.8 Sediment Accumulation Rate:
There is a high rate of sedimentation in the area of the slide. Large quantities of sediments are deposited annually at a rate of approximately 110 billion m/yr. (McKenna et al., 1992; Christian et al., 1994). It should be noted that, according to radioactive C14 dating accumulation rates at Sand Heads alone exceeds 18 cm per annum.

2.9 Subsurface stratigraphy to depth of slide plus 50% at the site adjacent to slide area (to predict pre-slide conditions):
The general soil profile of the Fraser River delta consists of three different layers. From the sea floor down to a depth of 21 m there is a variable sequence of clean fine sands and interbedded organic silts. From 21 m to 25 m, a denser zone of layered silty sands were encountered. Below these sands, to a depth of 30 m is a zone of regularly interbedded clean sands and silty sands (Christian et al., 1997).

2.10 Geotechnical Properties of slide sediments and surrounding stable material:

2.10.1 Shear strength: The undrained shear strength ranges from approximately 10 to 75 kPa to a depth of 100 m. This value was interpreted from a graph in Christian et al. (1998).

2.10.2 Water content: The water content of the soil ranges from approximately 10% to 50% as read from a graph in Christian et al. (1998).

2.10.3 Unit weight: The bulk density of the sediments range in value from 1.6 to 2.3 kg/m^3, as read from the graph in Christian et al. (1998). Also, it was assumed in Christian et al. (1994) that the effective unit weight of the soil was 6 kN/m^3.

2.10.4 Plasticity Index: The sediments in the Fraser River delta have a low plasticity value (Christian et al., 1997).

2.11 Possible releasing agents (indicate known or not):
Possible agents that may have caused the release of sediments are, the rapid deposition of sediments, the presence of interstitial gas, strong currents, waves and possibly earthquakes (Christian et al., 1997).

2.12 Nature of constant loads on the soil:
Wave loading effects have been demonstrated to be negligible (Luternauer & Finn, 1983; Christian et al., 1994).

2.13 Nature of variable loading on the soil:
Earthquake loading resulting in the strong shaking may trigger flow liquefaction on the steep slopes at the front of the delta (Christian et al., 1998).

2.14 Regional features (geohazards) and their effect on the slide:
A possible geohazard identified by GSC is the compressional creep-folding of weal sediments ahead of the prograding delta (Christian et al., 1998).

2.15 Evidence of tsunami generation:
It was suggested that if a major slide movement were to occur, an associated tsunami would be the result. However, there has yet to be any kind of evidence found to support this hypothesis (Hamilton & Wigen, 1987; Christian et al., 1994).

2.16 Reconstructed bathymetry of the site (if available):

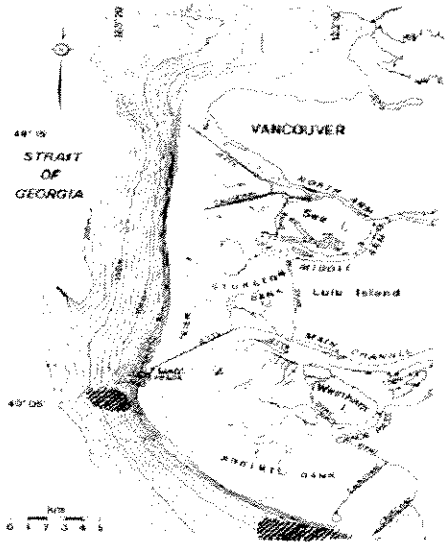

Figure A1.3: Fraser River Delta location map. (Luternauer et al., 1994)

References for Fraser Delta Slide:

Christian, H.A., Mosher, J.V., Barrie, J.V., Hunter, J.A. and Luternauer, J.L., 1998. Seabed slope instability on the Fraser River delta. *In*: Geology and Natural Hazards of the Fraser River Delta, British Columbia, (ed) J.J. Clague, J.L. Luternauer, and D.C.

Mosher; Geological Survey of Canada, Bulletin 525, p. 217-230.

Christian, H.A., Woeller, D.J., Robertson, P.K and Courtney, R.C., 1997. Site investigations to evaluate flow liquefaction slides at Sand Heads, Fraser River delta. Canadian Geotechnical Journal, v. 34 pp. 384-397.

Christian, H.A., Mudler, T., Courtney, R.C., Mosher, D.C., Barrie, J.V., Currie, R.G., Olynyk, H.W., and Monahan, P.A., 1994. Slope instability on the Fraser River Delta foreslope, Vancouver, British Columbia. 47th Canadian Geotechnical Conference, Halifax, N.S. September 21-23, pp. 155-165.

Hart, B.S., Prior, D.B, Barrie, J.V., Currie, R.G. and Luternauer, J.L, 1992. A river mouth submarine channel and failure complex, Fraser Delta, Canada. Sedimentary Geology, v. 81, pp. 73-87.

Hamiliton, T.S. and Wigen, S.O. 1987. The Foreslope Hills of the Fraser Delta: Implications for tsunamis in Georgia Strait. International Journal of the Tsunami Society, 5, pp. 15-33.

Hamilton, T.S. and Ricketts, B.D. 1994. Contour map of the sub-Quaternary bedrock surface, Strait of Georgia and Fraser Lowland; *In:* Geology and Geological Hazards of the Vancouver Region, Southwestern British Columbia, (ed.) J.W.H. Monger; Geological Survey of Canada, Bulletin 481, p. 193 – 196.

Hungr, O. 1993. Sandheads Lightstation risk assessment. Thurber Engineering Ltd. Report to the Canadian Coast Guard, Vancouver, B.C., February.

Luternauer, J. and Finn, W.D.L. 1983. Stability of the Fraser River Delta front. Canadian Geotechnical Journal, 20(4), pp. 603-616.

Luternauer, J.L.. Barrie, J.V., Christian, H.A., Clauge, J.J., Evoy, R.W., Hart, B.S., Hunter, J.A., Kileen, P.G., Kostaschuk, R.A., Mathewes, R.W., Monahan, P.A., Moslow, T.F., Mwenifumbo, C.J., Olynyk, H.W., Patterson, R.T., Pullan, S.E., Roberts, M.C., Robertson, P.K., Tarbotton., M.R., and Woeller, D.J., 1994. Fraser River delta: geology, geohazards and human impact; *In:* Geology and Geological Hazards of the Vancouver Region, Southwestern British Columbia, (ed.) J.W.H. Monger; Geological Survey of Canada, Bulletin 481, p. 197 – 220.

McKenna, G.T., Luternauer, J.L., and Kostaschuk, R.A. 1992. Large-scale mass-wasting events on the Fraser River delta front near Sand Heads, British Columbia. Canadian Geotechnical Journal, 29: 151-156.

Terzaghi, K. 1962. Discussion. On Sedimentation of Fraser River Delta, British Columbia. W.H. Mathews and F.P. Shepard, Bulletin of the American Association of Petroleum Geologists, 46(8), pp. 1438-1443.

Eureka (Humboldt) Retrogressive Slump

3.1 Location of slide and age of failure:

Figure A1.4: Location Map of Eureka Slide (Lee et al., 1981).

This slide took place on the continental margin, 30 km west of Eureka, California in the southern part of the Eel River basin. The Eel River basin extends from Cape Mendocino, California (40° 30' N) to Cape Sebastian, Oregon (42° 20' N). Within the basin the slide occurred just north of the Mendocino triple junction at the intersection of the Gorda, Pacific and North American plates. Gardner et al. (1999) reported the slide to have occurred between the late Pleistocene to the early Holocene period.

3.2 Detailed Bathymetry of site:

Figure A1. 3.2: Bathymetry of Eureka Site (Goff et al., 1999).

The slide lies within a shallow bowl-shaped depression. The depression is bounded by the self break on the east, by Little Salmon fault and an associated plunging to the north and a bathymetric high to the south. The main body of the slide is elongated with a length of about 10 km and an average thickness of 60 m (Gardner et al., 1999).

3.3 Type of Slide/Types of soil failure (slide, slump, mass flow, turbidity currents, etc.):

The failure is thought to be a shear dominated retrogressive movement occurring as a sequence of events. The central portion of the slide failed by extension creating folded and back-rotated blocks. This failure progressed up slope while the down slope style of deformation became compressional, creating folds in the slope sequence. As a late stage phenomenon, translational sliding is thought to have occurred at the top of the slide. The failure zone penetrates to a depth of about 65m below the sea floor (Gardner et al., 1999).

3.4 Failure Mechanism:

Progressive tectonic uplift near the shelf break steepened the slope angle and created a slope depression. This depression then became a depocentre for the high sediment flow from the Eel River. The high sediment accumulation rates result in a reduction of effective stress levels due to an increase in pore pressure. As well, pockmarks near the failure indicate that methane was generated from the decomposition of the organic carbon-rich sediment. The slope in the weakened state is then thought to be triggered to failure by short-term stresses generated by seismic activity (Gardner et al. 1999; Lee et al., 1981).

3.5 Geometry of Slide:

- 3.5.1 Amount of soil: 6 km^3 covering a 150 to 200 km^2 area (Gardner et al. 1999; Field and Edwards, 1981).
- 3.5.2 Depth of slide: 50 to 65 m (Gardner et al. 1999; Field, 1990).
- 3.5.3 Slope angle: 4° (Gardner et al. 1999; Field, 1990).
- 3.5.4 Run out Distance: 6 to 10 km (Gardner et al. 1999; Lee et al., 1981).
- 3.5.5 Water Depth: The slides are located at water depths of 250 to 500m (Field, 1990).

3.6 Slide Sediment Lithology:

The slide is mainly composed of silt. The sediment is noted as being gassy and comprised of enriched in plant and wood debris (Field and Edwards, 1981). The late Pleistocene and Holocene sediment is composed of thin-bedded turbidites of clayey silt and occasional thin sandy layers. (Gardner et al., 1999).

3.7 Degree of Consolidation:
All samples show some degree of overconsolidation (Lee et al., 1981).

3.8 Sedimentation Accumulation Rate:
Large quantities of sediment, approximately 20 to 30 x 10^6 tons per year, are delivered to the margin at a rate of about 1 to 7mm/yr (Field, 1990; Gardner *et al.* 1999).

3.9 Subsurface stratigraphy to depth of slide plus 50% at the site adjacent to slide area (to predict pre-slide conditions):
Four distinct sediment areas were sampled; (1) undisturbed sediment upslope from the slide, (2) disturbed sediment from the slide area, (3) undisturbed sediment downslope from the slide and (4) undisturbed sediment adjacent to the slide. Parameters obtained for each core location are; PI, both ω_L and ω_P and water content (Lee et al., 1981).

3.10 Geotechnical Properties:
- 3.10.1 Shear strength S_u: 2 to 36 kPa.
- 3.10.2 Water content: 35 to 60%
- 3.10.3 Bulk density ρ: 1.55 to 2.0 g/cc
- 3.10.4 Plasticity Index: 8.9 - 16.3% (Lee et al., 1981).

3.11 Nature of variable loadings on the soils:
- seismic
- rate of sedimentation
- tectonic uplift increasing the slope angle
- wave loading is negligible at water depth of 500 m where failure initially propagated (Lee et al., 1981).

3.12 Regional features and effects:
The continental margin off Northern California is known to have more landslides than any other region along the west coast of the United States. This area is recognized as having high levels of seismic activity, experiencing on average one event of magnitude 6 or greater per decade (Field, 1990).

Uplift areas of seafloor that are the result of tectonic forces surround the slide. The slide is bound at the north, southern and eastern perimeters with fault boundaries that progressively exhibit uplift. These uplifts steadily produce oversteepening of the slope and gradually increase the gravitational stresses acting on the slope.

The Eel River sediment outfall has both a high rate and is rich in organic matter. The organic matter decomposes and produces gas hydrates.

3.13 Source type and quality of data:
Cores:

Gravity corer, 3 m in length and 7.6 cm diameter (Lee et al., 1981). Box cores 20-60cm long and subsampled using a fixed piston device (Lee et al. 1999).

Geotechnical:

Miniature vane-shear tests, triaxial and consolidation tests were performed on gravity core samples retrieved by Lee *et al.* (1981).

Seismic and Sidescan:

Huntec DTS seismic-reflection profiles at 3.5 kHz at 540 joules towed at up to 500 m depth with subbottom penetrations up to 50 m and Datasonics SIS-1000 chirp sidescan-sonar at 100 kHz (simultaneous 1500 line km) (Gardner et al., 1999). The seismic grid executed by Gardner et al. (1999) was oriented by the Simrad EM-1000 multibeam bathymetry survey operating at 95 kHz with a maximum swath of 150° completed by Goff et al. (1999).

3.14 Reconstructed bathymetry of the site (if available):

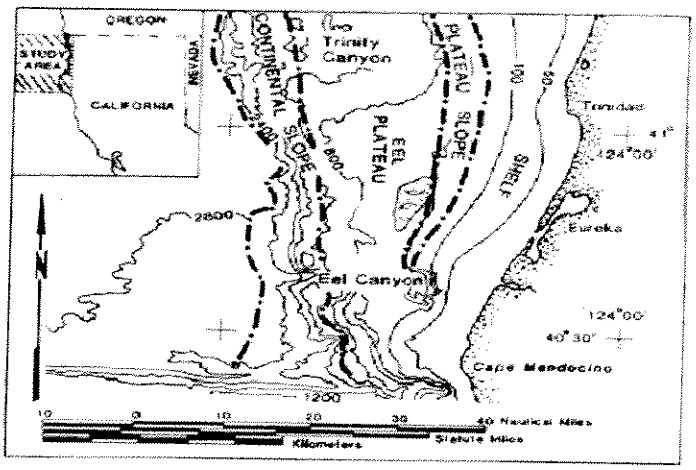

Figure A1.4: Location Map for Eureka Slide (Lee et al., 1981).

Huntec DTS seismic-reflection profiles at 3.5 kHz at 540 joules towed at up to 500 m depth with subbottom penetrations up to 50 m and Datasonics SIS-1000 chirp sidescan-sonar at 100 kHz (simultaneous 1500 line km) (Gardner et al., 1999). The seismic grid executed by Gardner et al. (1999) was oriented by the Simrad EM-1000 multibeam bathymetry survey operating at 95 kHz with a maximum swath of 150° completed by Goff et al. (1999).

3.14 Reconstructed bathymetry of the site (if available):

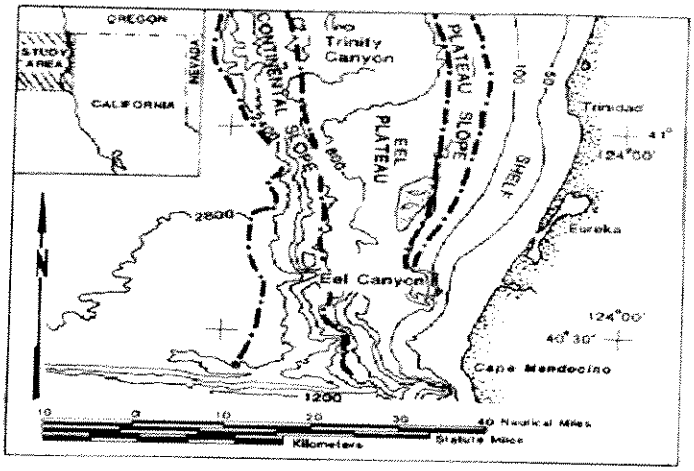

Figure A1.4: Location Map for Eureka Slide (Lee et al., 1981).

References for Eureka, California

Field, Michael E., 1990. Submarine Landslides Associated with Shallow and Gas Hydrates off Northern California. AAPG Bulletin, v74; 6, pp. 971-972.

Field, M.E. and Edwards, B.D., 1981. Large submarine slump off Eureka, California. AAPG Bulletin. 65; 5, pp. 924-925.

Gardner, J.V., Prior, D.B. and Field, M.E. (1999) Humboldt Slide – A Large Shear-Dominated Retrogressive Slope Failure, *Marine Geology*, Vol. 154, pp. 323-338.

Goff, J.A., Orange, D.L., Mayer, L.A. and Clarke, J.H. (1999). Detailed Investigation of Continental Shelf Morphology Using a High-Resolution Swath Sonar Survey: The Eel Margin, Northern California. *Marine Geology*, Vol. 154, pp. 255-269.

Lee, H.J., Edwards, B.D., and Field, M., 1981. Geotechnical analysis of a submarine slope, Eureka, California. Proceedings - Offshore Technology Conference. 13, Houston Texas. Vol. 4. pp. 53-65.

Lee, H.J., Locat, J., Dartnell, P., Israel, K. and Wong, F. (1999). Regional Variability of Slope Stability: Application to the Eel Margin, California. *Marine Geology*, Vol. 154, pp. 305-321.

Gulf of Cadiz Slide, Spain

4.1 Location of Slide and age of failure:
Figure A1.5: Location Map of the Gulf of Cadiz (Lee & Baraza, 1999).

The slide is located in the Gulf of Cadiz, Spain, northwest of Gibraltra Straight on the edge of the continental shelf (Lee and Baraza, 1999).

4.2 Detailed Bathymetry of site:
Figure A1. 6 (Baraza et al., 1999).

4.3 Type of Slide/ Type(s) of soil failure (slide, slump, mass flow, turbidity current, etc.):
Lee and Baraza (1999) suggest that the slump may correspond to a slump taking place in two phases. The first phase may have been the initiation of a retrogressive rotational slump while in the second phase the soil failed as a translational slide, leaving a fairly smooth seabed surface.

4.4 Failure Mechanism:
A possible triggering mechanism could be the oversteepening of the slopes due to erosion, leading to landsliding. Also, the presence of gas in the sediments of the Gulf of Cadiz may reduce the strength of the soil. This gas could also create a phenomena known as a blowout (a sudden escape of gas) that, if large enough, could result in sea-floor collapses (Baraza et al., 1999).

4.5 Geometry of Slide:

4.5.1 Amount of soil involved:

4.5.2 Depth of slide:
The total thickness of the submarine slides are 75 to 95 m (Baraza et al., 1999).

4.5.3 Slope angle:
The upper slope, to about 440 m water depth is very uniform at a gradient of 1.5°. The middle slope, from 440 to 600 m water depth, is less steep with slope angles ranging in general from 0.5 to 1° (Baraza et al., 1999).

4.5.4 Run out Distance:
There are a number of individual slumps that are from 200 to 750 m long (Lee and Baraza, 1999)

4.5.5 Water Depth:
The head of the slump lies in 157 m of water and the slide extends down to a depth of 440 m (Lee and Baraza, 1999).

4.6 Slide Sediment lithology:
The area of the slump is characterized by contorted and partially discontinuous internal reflectors with wavelengths of about 220 to 400 m within the more proximal and distal parts, and about 700 m within the central part of the slump (Lee and Baraza, 1999). There are representative boreholes for three different environments in the area of the slide: within the mapped submarine slump on the continental slope at a water depth of 275 m, on the continental slope but in unfailed sediment at 268 and 330 m water depth and on the continental shelf at 31 m water depth.

4.7 Degree of Consolidation:
Many of the soil samples were too course grained to allow the proper testing to obtain the maximum past stress. For the samples that did allow the consolidation test, the average estimated past stress was only 23 kPa. This value falls within the range usually associated with apparent rather than true overconsolidation. It appears that none of the samples showed the type of overconsolidation that results from sediment erosion or removal of overburden by mass wasting (Lee et al., 1981 *In*: Lee and Baraza, 1999).

4.8 Sediment Accumulation Rate: unknown

4.9 Subsurface stratigraphy to depth of slide plus 50% at the site adjacent to slide area (to predict pre-slide conditions):
Using high-resolution seismic data to a maximum penetration of 35 m, it can be shown that the slope is composed of parallel-bedded, weakly stratified and semi-transparent deposits (Lee and Baraza, 1999). Within the slump and on the continental slope adjacent to the slump the core samples consists of a 10 to 25 cm thick greenish brown, massive fine sand layer that lies above a sequence of mostly grey mud. Bioturbation is common throughout the mud and thin subhorizontal layers of slightly more course material along with dispersed bioclastic fragments, mainly mollusk shells. The core on the continental shelf appears to be composed of grayish olive mud with more frequent silty and sandy layers up to several cm thick. Below approximately 170 cm there seems to be a slightly courser material with common silty and sandy layers, and abundant shelly debris (Lee and Baraza, 1999).

4.10 Geotechnical properties of slide sediments and surrounding stable material:

4.10.1 Shear strength:
The vane shear strength near the surface of the cores varies between 2 and 15 kPa while the strength at depth 1.5 to 2 m varies between 5 and 10 kPa (Lee and Baraza, 1999).

4.10.2 Water content:
The water content of the sediment typically ranges between 25 to 80% throughout the whole study area. There appears to be no clear trend of decreasing water content with increased depth. The lowest water contents seem to occur at the surface and correspond to the courser sediment often found in the upper 30 to 50 cm (Lee and Baraza, 1999).

4.10.3 Unit weight:
Lee and Baraza (1999) used representative total unit weights of 1.709 g/cm^3 for the slump, 1.791 g/cm^3 for the continental shelf and 1.688 and 1.765 g/cm^3 for the continental slope outside of the slump material.

4.10.4 Plasticity Index:
Most of the samples fall within the CH field, suggesting that the sediments behave as inorganic soils of high plasticity. There was an exception of four samples from the shelf cores that show medium to low plasticity. Interpreting the plasticity index from Lee and Baraza (1999), the values range from approximately 26.5 to 56.2% and average 37.9%.

Other:

4.10.5 The friction angle ranges from 21 to 41° within the study area (Lee and Baraza, 1999).

4.11 Possible releasing agents (indicate known or not):

It appears from seismic profiles that surficial slumping tends to be associated with gassy sediment. Also, there is probably active gas seepage at some slope locations (Baraza and Ercilla, 1996 *In*: Lee and Baraza, 1999).

4.12 Nature of variable loads on the soils:

Fluctuations in the shear stress can be caused by storm waves or earthquakes. This can result in an increase in pore water pressure, which decreases the shear strength of the sediment (Lee and Edwards, 1986; Lee and Baraza, 1999).

4.13 Regional features (geohazards) and their effect on the slide:

The slump displays a step-like internal structure which denotes weakly developed shear planes within the soil. Also, there is evidence of gas within the surficial sediment as observed on seismic records (Lee and Baraza, 1999). The area is located near a continental margin where the African and Eurasian plates are converging at a rate of 2-3 mm/yr. This makes the Gulf of Cadiz very susceptible to seismic activity that could result in many offshore instability processes such as submarine landslides (Baraza et al., 1999).

4.14 Evidence of tsunami generation:

There are records of numerous submarine slides occurring in the Gulf of Cadiz, some of which did have an accompanying tsunami (Baraza et al., 1999).

4.15 Reconstructed bathymetry of the site (if available):

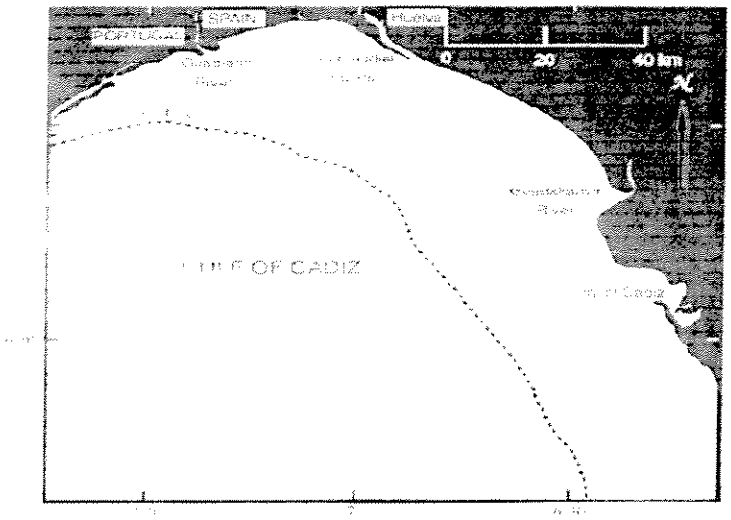

Figure A1.5: Location Map of Gulf of Cadiz, Spain (Lee and Baraza, 1999).

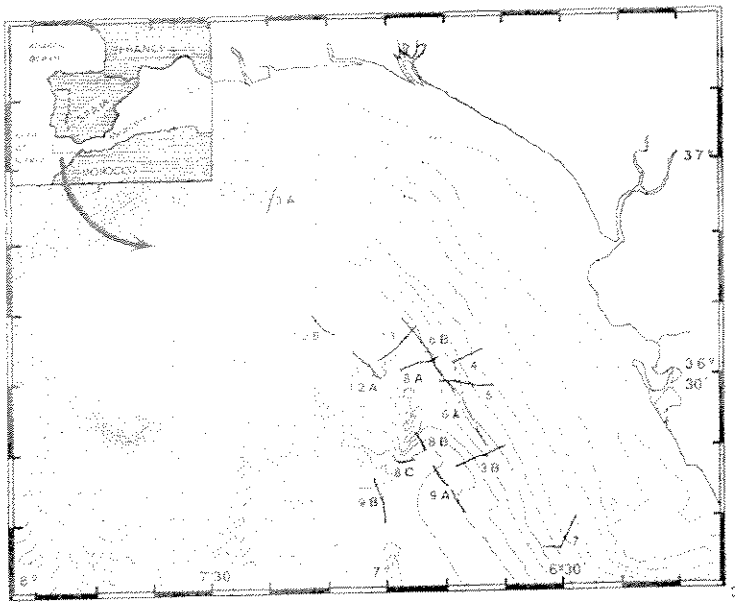

Figure A1.6: Bathymetry of Gulf of Cadiz (Baraza et al, 1999)

References for the Gulf of Cadiz, Spa

Baraza, J., Ercilla, G. and Nelson, C.H., 1999. Potential Geologic hazards on the eastern Gulf of Cadiz slope (SW Spain). Marine Geology, v. 155, pp. 191-215.

Baraza, J. and Ercilla, G., 1996. Gas-charged sediments and large pockmark-like features on the Gulf of Cadiz (SW Spain). Mar. Pet. Geol. 13. 253-261.

Lee, H. and Baraza, J, 1999. Geotechnical characteristics and slope stability in the Gulf of Cadiz. Marine Geology, v. 155, pp. 173-190.

Lee, H.J. and Edwards, B.D., 1986. Regional method to assess offshore slopes stability. Journal of Geotechnical Engineering, American Society of Civil Engineers, 112, 489-509.

Lee, H.J., Edwards, B.D., Field, M.E., 1981. Geotechnical analysis of a submarine slump, Eureka, California. Proc. 13th Annual Offshore Technol. Conf., Houston, TX, pp. 53-59.

Kahe Point, Oahu Slide, Hawaii (Hurricane Iwa related)

5.1 Location of Slide and age of failure:
Figure A1.7: Location Map of Oahu Slide, Hawaii (Tsutsui et al., 1981).

A submarine slide occurred off the coast of Hawaii, just west of the Island of Kauai on November 23, 1982 (Normark et al., 1993).

5.2 Detailed Bathymetry of site:
Figure A1.8 Bathymetry of Oahu Slide (Normark et al., 1993).

5.3 Type of Slide/ Type(s) of soil failure (slide, slump, mass flow, turbidity current, etc.):

Turbidity currents and/or slumps appear to have resulted from the large storm-generated waves off the coast of Oahu, Hawaii. This soil failure can be proven by the movement of current sensor moorings, located along a proposed pipeline route, downslope. It is believed that hurricane Iwa generated a series of slump events that resulted in the creation of turbidity currents. These currents are responsible for the movement of the moorings (Dengler et al, 1984).

5.4 Failure Mechanism:
It is believed that rapid loading and unloading of the slope sediment due to the large hurricane-induced storm waves moving over the area could have caused a significant loss of strength within the sediment. This reduction in strength would have generated downslope directed forces to move the sediment (Normark et al, 1993). Noda (1983) suggested that the strong currents produced by the advancing storm could have eroded and put into suspension sufficient sediment to generate a turbidity current directly (Normark et al., 1993).

5.5 Geometry of Slide:

5.5.1 Amount of soil involved:
No quantitative estimate of the total amount of material loss from the shelf area was made, but an observation by HECO divers indicate that most of the reef surface was swept clean of sediment (Tsutsui et al., 1987).

5.5.2 Depth of slide:
The displaced moorings were originally located 10 m above the sea floor, implying that the mass flow was at least 10 m thick (Normark et al., 1993).

5.5.3 Slope angle:
Immediately offshore from Kahe Point, the shelf is narrow and steep at an average slope of 30 to 40°. Farther offshore, at a water depth of approximately 1500 m, the slope increases to about 20° (Normark et al., 1993).

5.5.4 Run out Distance:
Sensors located on the slope were recorded as having total water depth changes of up to 220 m, which translates to downslope movement as much as 2.4 km (Dengler et al., 1984)

5.5.5 Water Depth:

Movement of soil and telecommunication cables was observed in water depths greater than 1,100 m (Chui et al., 1983; Normark et al., 1993).

5.6 Slide Sediment lithology:

The general area appears to be composed of predominantly silt and clay sized sediment. There are areas comprised of poorly sorted, angular, coarse sand and gravel with a minimum thickness of 2.5 m. The shallowest telecommunication cable was broken and partially buried in the area immediately downslope from where two zones of course sediment converge. This evidence suggests it is likely that some, or perhaps all, of this coarser sediment was displaced (through slumping and turbidity currents) during Hurricane Iwa (Normark et al., 1993).

5.7 Degree of Consolidation: unknown.

5.8 Sediment Accumulation Rate: unknown.

5.9 Subsurface stratigraphy to depth of slide plus 50% at the site adjacent to slide area (to predict pre-slide conditions):

Most of the study area seems to consist of a relatively thick upper sequence of fine-grained sediment overlaying coarse-grained layer. This top layer is composed of moderately sorted, medium to fine silt with a thickness ranging from 200 to 380 cm, averaging 300 cm. These layers are usually covered by clay and silt sized sediment (Tsutsui et al., 1987).

5.10 Geotechnical properties of slide sediments and surrounding stable material:

5.10.1 Shear strength: No data available.

5.10.2 Water content: No data available.

5.10.3 Unit weight:

The density difference between the turbidity current and the ambient water is given a theoretical upper limit and an empirical lower limit. It is suggested that the theoretical upper limit reaches 0.15 g/cm^3, while the empirical lower limit is 0.0005 g/cm^3. A typical range found in turbidity currents is 0.003 to 0.11 g/cm^3 (Bagnold, 1954 *In*: Dengler et al., 1984).

5.10.4 Plasticity Index:

5.11 Possible releasing agents (indicate known or not):

It was suggested that several debris flows triggered by rapid changes in pore pressure due to the hurricane-induced waves were responsible for the array movements and deep-water cable damage (Hollister, 1984; Tsutsui et al., 1987). Fornari (1984) found no evidence of recent bedrock movement and therefore suggested that slumping is not responsible for the events recorded during the passage of Hurricane Iwa. He believed that the damage to the cables was caused by breaking internal waves (Tsutsui et al., 1987).

5.12 Nature of constant loads on the soils:

5.13 Nature of variable loads on the soils:

Rainfall in the study area is primarily orographic and the coastline is relatively arid. There are few streams in this area, therefore flow and sediment discharge from rivers into the offshore environment occurs only after infrequent storms (Maragos, 1979; Tsutsui et al., 1987). Sediment deposits are largest and thickest directly off Kahe Point, which is the area of the hurricane-induced submarine slide (Tsutsui et al., 1987). Tsutsui et al. (1987) suggest that events such as Hurricane Iwa, which lead to submarine slope failures, may occur as frequently as every 5-7 years, the approximate recurrence interval for an El Nino related hurricane event. This interval could be even shorter if you include the possibility of other major events such as earthquakes and tsunamis, which could also trigger submarine slides and turbidity currents.

5.14 Regional features (geohazards) and their effect on the slide:
There are several volcanoes in the study area. Slumping of volcanic bedrock has been used to explain the irregular bathymetric configurations off portions of Oahu and the other various Hawaii submarine slopes (Tsutsui et al., 1987).

5.15 Evidence of tsunami generation:
Hurricane Iwa generated waves at a significant wave height of 5 m, with a maximum height of 9 m (Noda, 1983; Dengler et al., 1984).

5.16 Reconstructed bathymetry of the site (if available):

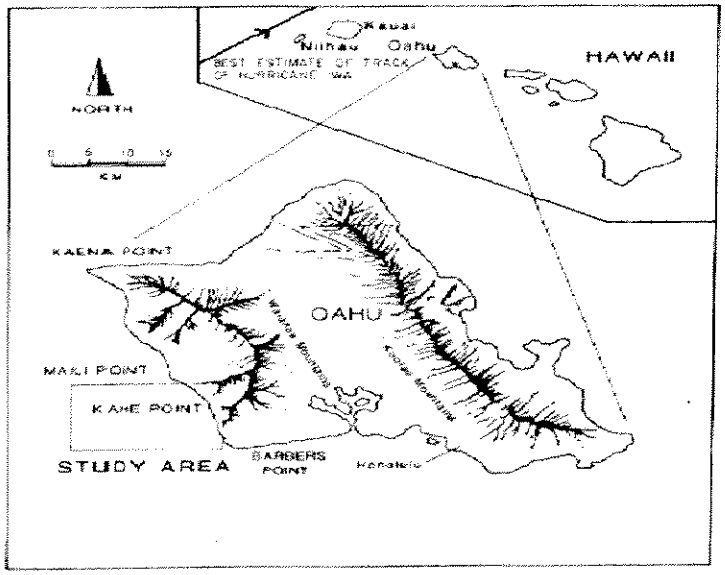

Figure A1.7: Location map, Kahe Point, Oahu Slide, Hawii (Tsutsui et al, 1981)

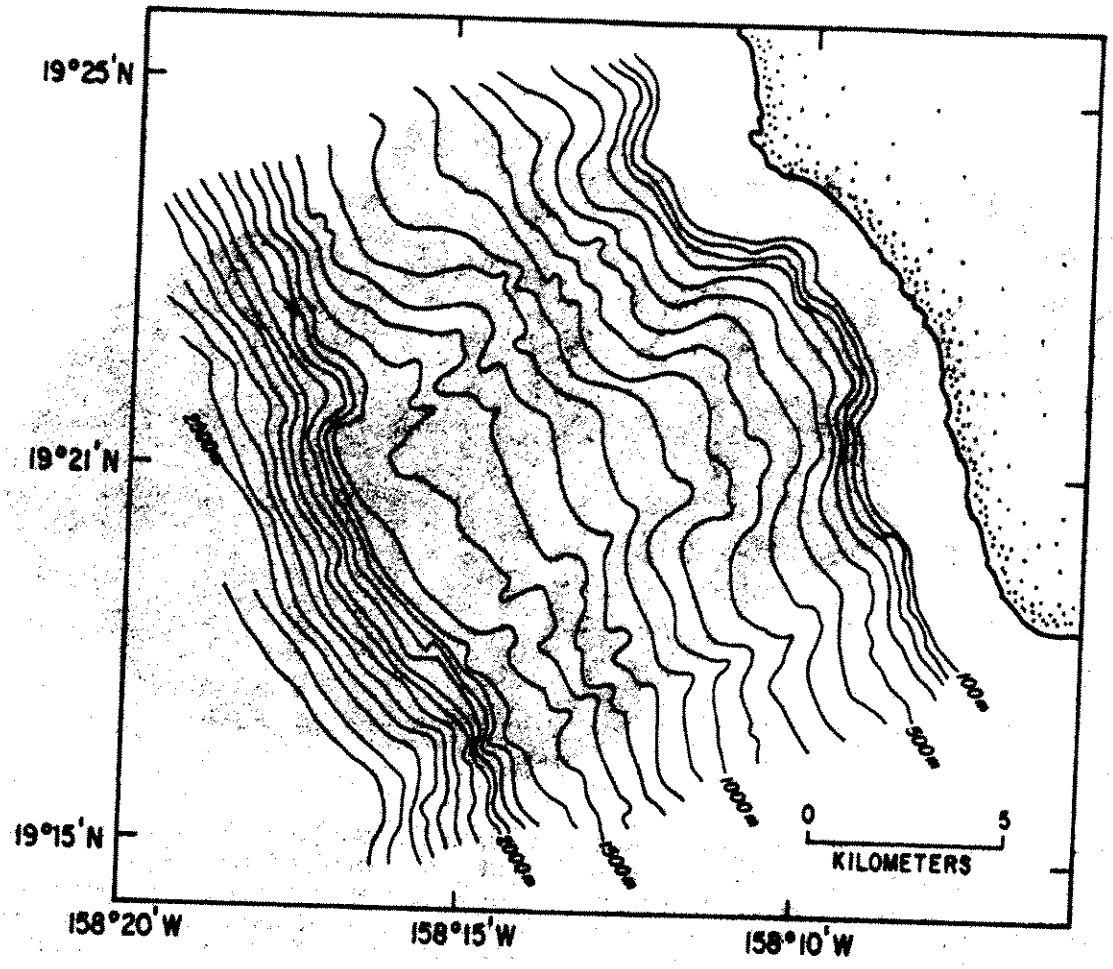

Figure A1.8: Oahu Slide Bathymetry (Normark et al, 1993).

References for Hawaii (Hurricane Iwa related)

Bagnold, R.A., 1954. Experiments on a Gavity-free dispersion of large solid spheres in a Newtonian Fluid under shear. Proceedings of the Royal Society of London, 225, pp. 49-63.

Chui, A.N.L., Escalante, L.E., Mitchell, J.K., Perry, D.C., Schroeder, T.A., and Walton, T., 1983. Hurricane Iwa, Hawaii, November 23, 1982: National Academy Press, Washington, D.C., p. 68.

Dengler, A.T., Noda, E.K., Wilde, P. and Normark, W.R., 1984. Slumping and related turbidity currents along proposed OTEC cold-water-pipe route resulting from Hurricane Iwa: Proceedings of the 1984 Offshore Technology Conference, Houston, Texas, OTC 4702, p. 475-480.

Fornari, D.J., 1984. Preliminary report: SeaMARC II side-scan sonar image of the seafloor off Kahe Pt., Oahu, Hawaii. Offshore Investigations Ltd., Chatham, N.Y., pp.14.

Hollister, C.L., 1984. Cable failures off Oahu, Hawaii caused by Hurricane Iwa. Woods Hole Oceanogr. Inst., Tech. Rep., WHOI 84-31, pp. 26.

Maragos, J.E., 1979. Oahu Coral Reef Inventory. Report for U.S. Army Corps of Eng., Honolulu, Hawaii, pp. 379.

Noda, E.K., 1983. Effects of Hurricane Iwa, November 23, 1982, offshore of Kahe Point, Oahu: Technical Report for Research Corporation, University of Hawaii, Honolulu, Hawaii, p. 56.

Normark, W.R., Wilde, P., Campbell, J.F., Chase, T.E. and Tsutsui, B, 1993. Submarine Slope Failures Initiated by Hurricane Iwa, Kahe Point, Oahu, Hawaii. *In*: Submarine Landslides: Selected Studies in the U.S. Exclusive Economic Zone. (ed) Schwab, W.C.,

Lee, H.J. and Twichell, D.C. U.S. Geological Survey Bulletin 2002, pp. 197-204.

Tsutsui, B, Campbell, J. F. and Coulbourn, W.T., 1987. Storm-Generated, Episodic Sediment Movements off Kahe Point, Oahu, Hawaii. Marine Geology, v. 76, pp. 281-299.

APPENDIX 2: THE ROLE OF EARTHQUAKES IN TRIGGERING SUBMARINE SLIDE FAILURES

Earthquakes are considered to be one of the most effective release mechanisms and are known to have triggered major submarine slides all over the world, see Table A2.1. In areas with minor sedimentation at present, earthquakes are the most important release factor for natural submarine slides. Vibrations caused by explosions and/or blasting can have similar effects on the soil as earthquakes and should also be considered as a possible release mechanism. The different earthquake-induced load effects that could make a submarine slope unstable and trigger a slide are discussed below.

Liquefaction phenomenon

Generally, liquefaction-susceptible sediments, such as silt and loose sand, are most vulnerable to earthquakes. The phenomenon of liquefaction is related to rapid build-up of the pore water pressure. During the shaking, the loose sand/silt tends to compact. The water in the pores cannot escape quickly enough to accommodate instantaneously the compaction. Therefore the stresses are thrown on the water, increasing the pore water pressure. This leads to a reduction in the effective stress and loss of soil shear strength, with potentially dramatic consequences.

Most of the deepwater sites, however, consist of clay or clayey sediments. The critical parameters for clay to have a potential for liquefaction were studied by Seed et al. (1983) who state:

> *Both laboratory tests and field performance data have shown that the great majority of clayey soils will not liquefy during earthquakes. However, recent studies in China have shown that certain types of clayey materials may be vulnerable to severe strength loss as a result of earthquake shaking. These soils appear to have the following characteristics:*
>
> | | | |
> |---|---|---|
> | *Percent finer than 0.005 mm* | < | *15%* |
> | *Liquid limit* | < | *35%* |
> | *Water content* | > | *0.9 x liquid limit* |

If soil layers with high liquefaction potential are identified within the sediments, a detailed evaluation would be required to estimate the risk of liquefaction and slide initiation under the design earthquake event. The most common procedures for evaluation of liquefaction potential are summarised in Kramer (1996), TC4-ISSMGE (1999), and Robertson and Fear (1995).

Table A2.1 Earthquake induced submarine slides (NGI, 1997)

Slide	age/date	V (m^3)	L/H	L (km)	H (m)	Soil	Trigger	Damage
Bassein, Bay of Bengal	ancient	700 to 900 x 10^9	98	215	2200	-	combination of sedimentation and earthquake	
Storegga, Norway	ancient	800 x 10^9	94	160	1700	-	possibly earthquake induced	severe flooding
Grand Banks	1929	760 x 10^9	150	750	5000	sand, silt	earthquake	cable breaks
Bjørnøya, Norway	ancient	500 x 10^9	80	200	2500		possibly earthquake induced	
Alika, Hawaii	holocene/ pleistocene	200 to 500 x 10^9	83	250	3000	basalt	earthquake	
Nice, France	1979	> 100 x 10^9	167	> 250	1500	clayey silt	earthquake, tsunami	destruction of buildings, coastal structures, cable breaks
Ice bay/Malaspina, Gulf of Alaska	recent/ pleistocene	32 x 10^9	150	12	80	clayey silt	earthquake	
Copper river, Gulf of Alaska	recent/ pleistocene	24 x 10^9	94	8	85	silty clay	rapid sedimentation and possibly earthquake/free gas/wave loading	
Ranger, Baja California	ancient	20 x 10^9	46	37	800	clayey and sandy silt	sedimentation and possibly earthquake induced	
Albatross bank, Gulf of Alaska	recent/ pleistocene	19 x 10^9	9	5.3	600	silty clay	combination of earthquake and oversteepening	
Sagami Bay	1923	10 x 10^9	-	350	-	-	earthquake	cable breaks
Kidnappers, New Zealand	ancient	8 x 10^9	55	11	200	sandy silt and clay	possibly earthquake induced	
Kayak trough, Gulf of Alaska	ancient	5.9 x 10^9	120	18	150	silty clay	combination of sedimentation and earthquake	
Paoanui, New Zealand	ancient	1 x 10^9	35	7	200	silt/sand	possibly earthquake induced	
Isfjorden, Svalbard	ancient	0.5 to 1 x 10^9	17	30	1800?		possibly earthquake induced	
Messina	1908	>> 10^6	69	220	3200	sand, silt	earthquake/tsunami/seiche	destruction of buildings, coastal structures, cable breaks
Orleansville	1954	>> 10^6	38	100	2600	-	rapid sedimentation and earthquake	cable breaks
California	ancient	250 x 10^6	23	3.5	150	clayey and sandy silt	possibly earthquake induced	
Suva, Fiji	1953	150 x 10^6	61	110	1800	sand	earthquake/tsunami/seiche	destruction of buildings, coastal structures, cable breaks
Valdez, Alaska	1964	75 x 10^6	8	1.28	168	gravelly silty sand	earthquake	
Scripps canyon	1949/50	1 x 10^6	11	2	175	-	earthquake and hurricane waves	
Storglomvatn, Norway	1989	10 x 10^3	15	3	200		explosives, field experiment	
Kenai Lake, Alaska	1964	1 x 10^3	3	1.5	500	-	earthquake/tsunami/seiche	destruction of buildings
Mid Atlantic ridge	-	-	-	10	-	-	earthquake/tsunami/seiche	
Port Royal, Jamaica	1692	-	-	-	-	-	earthquake/tsunami/seiche	approx. 2000 people killed
Chile	1922	-	-	-	-	-	earthquake/tsunami/seiche	destruction of buildings and coastal structures
Amorgos/Aegean, Greece	1956	-	-	-	-	-	earthquake/tsunami/seiche	destruction of buildings and coastal structures
Hebgen Lake, Montana	1959	-	-	-	-	-	earthquake	casulties
Markham river delta	1966/68	-	-	-	-	-	earthquake	casulties, cable breaks
Solomon sea	1970/71	-	-	-	-	-	earthquake/tsunami/seiche	

Temporary mobilisation of shear strength and cyclic degradation

Even though most of the deepwater sediments could be considered to have a low liquefaction potential, they might still develop into a slide when subjected to a strong earthquake. Earthquakes generate vibrations and mass inertia forces, which at times cause large shear stresses in the down-slope direction. However, the load duration is short and in most situations, the main effects are accumulation of down-slope displacements and cyclic degradation of strength.

The evaluation of slope stability under earthquake loading is commonly based on pseudo-static analyses. In a pseudo-static analysis, the inertial force caused by ground acceleration is applied as an effective static load equal to the mass of soil times the peak or the effective acceleration. Consider a very long, submerged clay slope. The static shear stress on a plane parallel to the seabed is:

$$\tau_{static} = \gamma' \cdot h \cdot \cos\theta \cdot \sin\theta$$

where γ' = submerged unit weight
h = depth below seabed
θ = slope angle

If the slope is subjected to an up-slope acceleration "a" parallel to the seabed, it will experience additional shear stress due to the down-slope mass inertia force (note that the inertia force acts in the opposite direction to acceleration) on the plane at depth h:

$$\tau_{dynamic} = \gamma \cdot h \cdot \cos^2\theta \cdot a/g$$

where γ = total unit weight
g = gravitational acceleration = 9.81 m/s^2

The pseudo-static safety factor for the clay slope is the undrained shear strength at depth h divided by the sum of driving shear stresses. For a normally consolidated slope, the undrained shear strength may be assumed to be proportional to the effective normal stress on the plane, i.e.

$$s_u = b \cdot \gamma' \cdot h \cdot \cos^2\theta$$

where s_u = undrained shear strength at depth h
b = ratio of undrained shear strength to effective normal stress

Thus the pseudo-static safety factor is:

$$FS = \frac{s_u}{\tau_{static} + \tau_{dynamic}} = \frac{b}{\tan\theta + \frac{a}{g} \cdot \frac{\gamma}{\gamma'}}$$

A typical set of parameters for normally consolidated clay would be b = 0.25, γ = 17 kN/m^3, and γ' = 7 kN/m^3. With these parameters and a slope angle of θ = 5°, an up-slope acceleration of 0.067g

reduces the safety factor to 1.0. For $\theta = 10°$, an up-slope acceleration as low as 0.03g does the same.

The safety factor obtained from a pseudo-static analysis is not always a useful measure for evaluating the seismic response of a slope. A pseudo-static safety factor less than unity during the peak earthquake-induced load does not necessarily indicate slope failure with large movement of soil masses. The maximum earthquake loads only last a fraction of a second and, as long as the soil does not experience a dramatic reduction of shear strength, the consequence of full mobilisation of soil shear strength along a slip surface will be limited permanent deformations. The ground acceleration which gives a factor of safety of unity in the pseudo-static analysis is called the cut-off acceleration. If a slope is subjected to an earthquake with a peak acceleration higher than the cut-off value, permanent deformations along the slip surface will take place. In his Rankine Lecture, Newmark (1965) presented the sliding block model for computing the seismically-induced permanent displacements in dams, embankments, and slopes. Newmark developed equations and a chart for predicting the permanent relative displacements induced by earthquakes.

The key questions regarding the stability of a clay slope under a strong earthquake are:

- Will the soil mass experience essentially elastic deformations during the earthquake, or will non-reversible, plastic deformations occur? If plastic deformations do occur, how large will the permanent displacements be?
- Will the earthquake loading trigger creep of the slope leading to large shear displacements after the earthquake?
- Will the soil keep its shear strength after being exposed to the high cyclic shear stresses induced by the earthquake, or will it lose so much of its strength that a slide develops. The latter situation would be the case if, for example, liquefaction takes place.

To answer these questions, NGI has been developing earthquake response analysis procedures (Nadim et al., 1996) and executing special laboratory testing program on marine clays (Nadim and Kalsnes, 1997) since the mid 90's. The purpose of the special laboratory testing program is to investigate the influence of the following factors on the shear strength of a soil element within a slope:

- rapid rate of loading,
- permanent (static) shear stress on the potential failure surface,
- cyclic loading induced by earthquake ground motion,
- creep deformations after the earthquake, and
- post-earthquake static shear strength

The first two factors tend to **increase** the undrained shear strength. For example, the special laboratory tests performed on undisturbed soil samples from Fensfjord in west Norway showed that, due to rapid rate of loading, the cyclic shear strength under earthquake loading was 60 – 80% greater than the static shear strength (Nadim et al., 1996).

On the other hand, the cyclic shear strains induced by the earthquake tend to **reduce** the shear strength. If the earthquake-induced cyclic shear strains are large, the slope could undergo further creep displacements after the earthquake and experience a significant reduction of static shear strength. Figure A2.1 shows a summary of the results of some of the special tests performed on soft Norwegian marine clays (Nadim and Kalsnes, 1997). It can be seen that for the type of material tested, creep strains and reduction of static shear strength become significant when the earthquake-induced cyclic shear strain exceeds 1 – 2%.

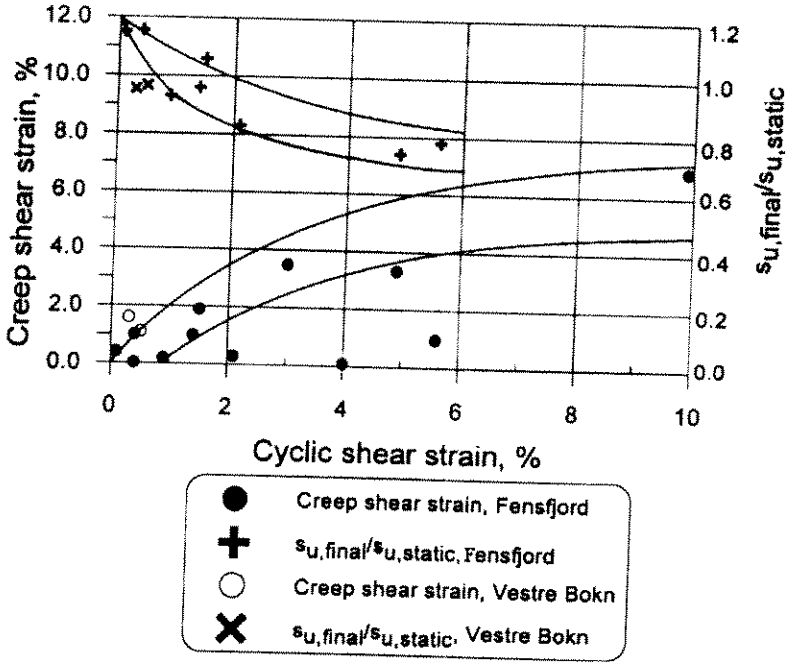

Figure A2.1: Trends of creep strain after 24 hours and reduction in static undrained shear strength as functions of maximum cyclic shear strain during cyclic testing.

However, analytical simulations of the seismic response of submarine slopes comprised of deep clay sediments have shown that if the soil profile is more-or-less uniform, then the earthquake-induced cyclic shear strain rarely exceeds 0.5%. These simulations show that the peak seabed displacement and the maximum earthquake-induced shear strain within the soil profile increase rapidly as the slope angle increases. This increase is due to the accumulation of irreversible (permanent) shear strains in the down-slope direction.

The earthquake-induced cyclic shear strains are far below the levels that might lead to significant degradation of shear strength. Figure A2.2 shows a typical computed shear stain time history within a critical layer in a slope subjected to very strong shaking (NGI, 1999). It can be seen that the ground motion causes large accumulated shear strains in the down-slope direction, while the amplitude of the individual shear strain cycles is relatively modest.

On the other hand, the cyclic shear strains induced by the earthquake tend to **reduce** the shear strength. If the earthquake-induced cyclic shear strains are large, the slope could undergo further creep displacements after the earthquake and experience a significant reduction of static shear strength. Figure A2.1 shows a summary of the results of some of the special tests performed on soft Norwegian marine clays (Nadim and Kalsnes, 1997). It can be seen that for the type of material tested, creep strains and reduction of static shear strength become significant when the earthquake-induced cyclic shear strain exceeds 1 – 2%.

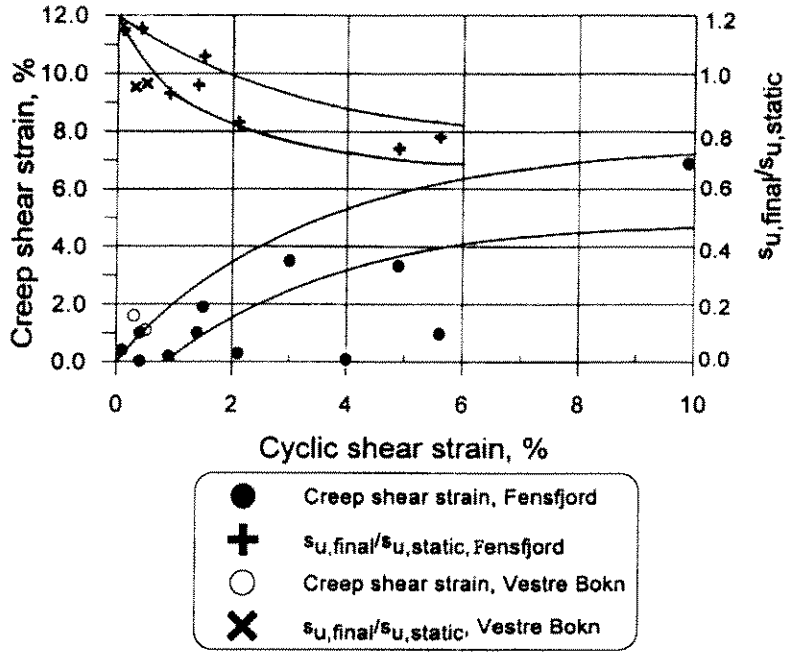

Figure A2.1: Trends of creep strain after 24 hours and reduction in static undrained shear strength as functions of maximum cyclic shear strain during cyclic testing.

However, analytical simulations of the seismic response of submarine slopes comprised of deep clay sediments have shown that if the soil profile is more-or-less uniform, then the earthquake-induced cyclic shear strain rarely exceeds 0.5%. These simulations show that the peak seabed displacement and the maximum earthquake-induced shear strain within the soil profile increase rapidly as the slope angle increases. This increase is due to the accumulation of irreversible (permanent) shear strains in the down-slope direction.

The earthquake-induced cyclic shear strains are far below the levels that might lead to significant degradation of shear strength. Figure A2.2 shows a typical computed shear stain time history within a critical layer in a slope subjected to very strong shaking (NGI, 1999). It can be seen that the ground motion causes large accumulated shear strains in the down-slope direction, while the amplitude of the individual shear strain cycles is relatively modest.

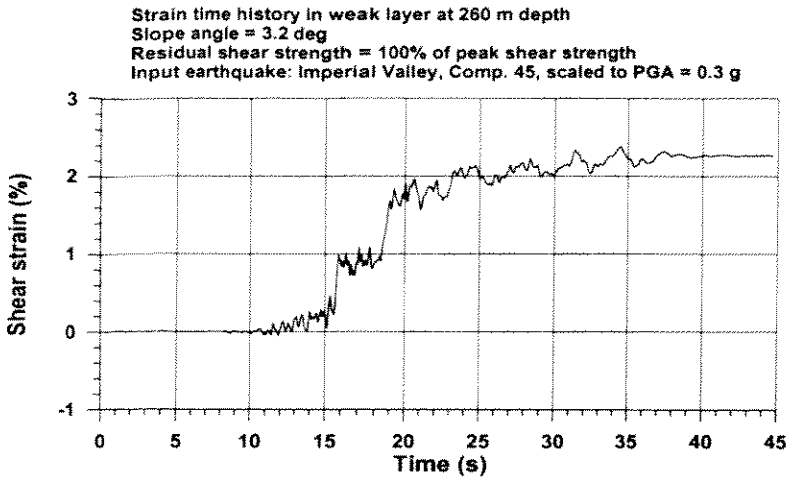

Figure A2.2 Time history of strain in an assumed weak layer at 260 m depth for 10^{-4}/year earthquake event (see NGI report 981225-2).

In a study of sea floor stability in the Seabed Project (NGI, 1999) sensitivity analyses were performed to evaluate the effects of a weak, soft layer on the seismic slope stability. The conclusion drawn from those analyses was that **a weak, soft soil layer with strong degradation of shear strength beyond the peak strength could lead to slope instability under earthquake loading**. The analyses also showed that low shear modulus is just as important as the low residual strength of the weak layer in initiating earthquake-induced instability. In future site investigations, one should focus on identifying anomalous layers with much lower shear modulus (or shear wave velocity) than the neighbouring layers, as well as layers with unusually low shear strength. Figure A2.3 shows the results of two simulations from the NGI (1999) study. The effects of a weak layer at a depth of 260m on the shear strains induced by a 10,000-year earthquake event can clearly be seen in the figure. Without the weak layer, the maximum shear strain occurs near the seabed and is about 0.3 – 0.4%. In presence of a soft, weak layer, the earthquake-induced strains tend to concentrate in that layer and a maximum shear strain of over 3% might occur.

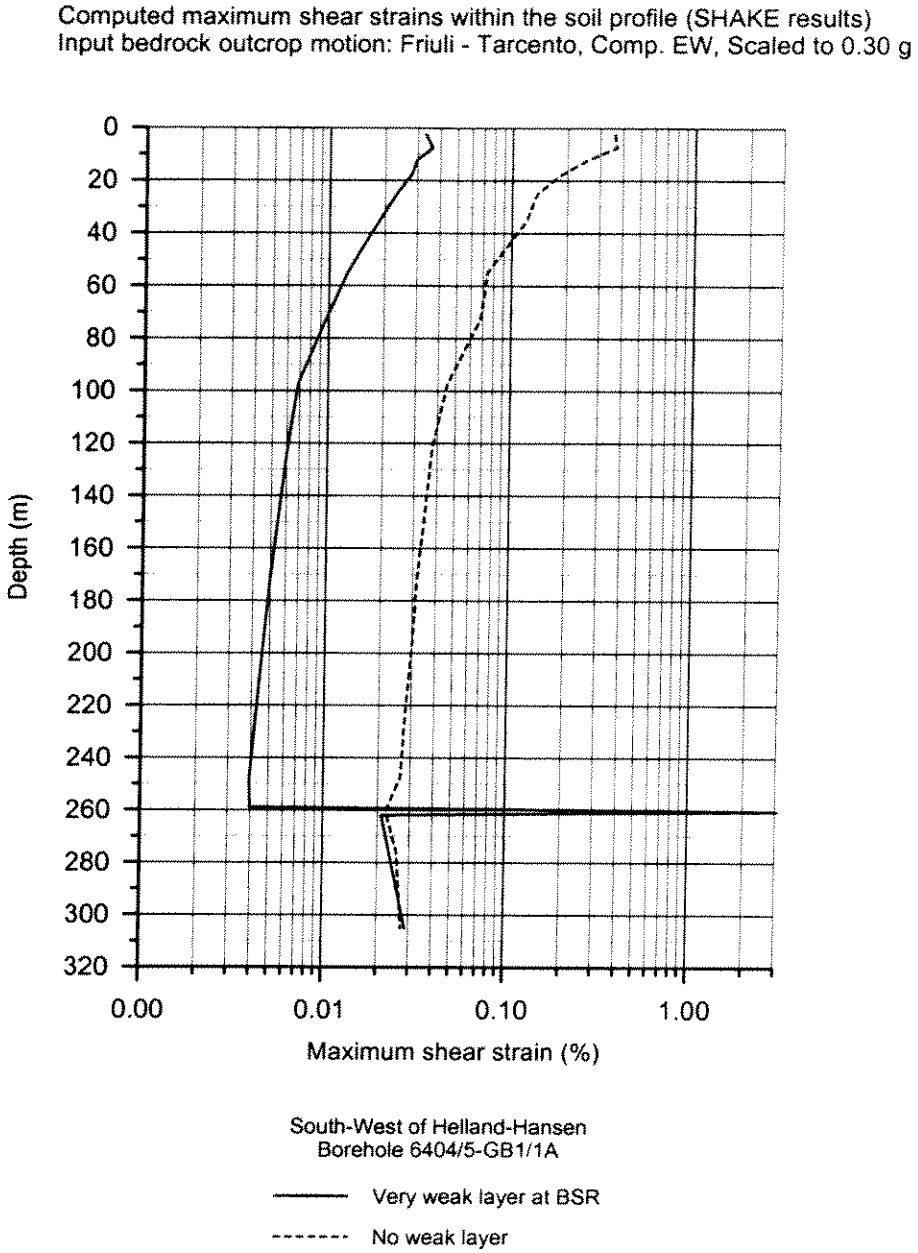

Figure A2.3 Maximum earthquake-induced shear strain within a soil profile with and without assumed weak layer at 260 m depth for 10^{-4}/year earthquake event (see NGI report 982512-2).

Current research at NGI (Pestana and Nadim, 2000) has identified another earthquake-related mechanism that might lead to failure of a submarine clay slope. A strong earthquake generates excess pore pressures within the soil profile. Following the earthquake, the excess pore pressures dissipate towards the seabed. If a soil layer at a critical location has significantly lower permeability than the layers below, then excess pore pressure in that layer might **increase** with time, leading to a reduction of effective stresses and lower shear strength, and possibly slope failure.

To illustrate this mechanism, a 100 m thick, normally consolidated soft clay deposit with the shear modulus and shear wave velocity profiles shown on Figure A2.4 was considered. Figure A2.5 shows the predicted excess pore pressures subjected to a strong earthquake The earthquake-induced excess pore pressures were estimated using a new, simple soil model which captures the most important features of clay response under seismic loading (Pestana, 2000). Figure A2.6 shows the dissipation of the excess pore pressures (normalised with respect to the in situ effective vertical stress) with time in a uniform soil profile (Scenario A). It can be seen that for Scenario A, the highest pore pressure ratio (i.e. highest relative reduction in effective stress and shear strength) occurs close to the sea bed immediately after the earthquake. Figure A2.7 shows the dissipation of the excess pore pressures with time when the permeability of the soil layer at 5 m depth is 100 times lower than the permeability of neighbouring layers (Scenario B). It can be seen that in this situation, the very low permeability layer acts as a barrier for the dissipation of excess pore pressures from the deeper layers towards the sea bed. This leads to a significant increase in pore pressure in that layer for a long time after the earthquake event. The maximum reduction in the effective stresses and shear strength of the low permeability layer occurs after about one year. The reduction of the shear strength due to the pore pressure build-up could lead to slope failure and slide initiation if slope is marginally stable prior to earthquake.

Figure A2.8 shows schematically the effective stress paths predicted by the new soil model (Pestana, 2000) in monotonic undrained loading. The zone labeled as "potentially unstable" is the zone where the shear strength mobilization is so high that the slope might fail because of creep. Figures A2.9 through A2.11 summarize the different earthquake-induced load effects that could fail a submarine clay slope and develop it into a slide. The stress paths for a typical soil element on the slip plane are shown for 3 scenarios:

Scenario 1 – Failure occurs during the earthquake. Soil has strong strain-softening characteristics and high sensitivity. The strains and pore pressures generated by the cyclic stresses degrade the shear strength so much that the slope is not able to carry the static shear stresses.

Scenario 2 – Post-earthquake failure due to increase in excess pore pressure caused by seepage from deeper layers.

Scenario 3 – Post-earthquake failure due to creep.

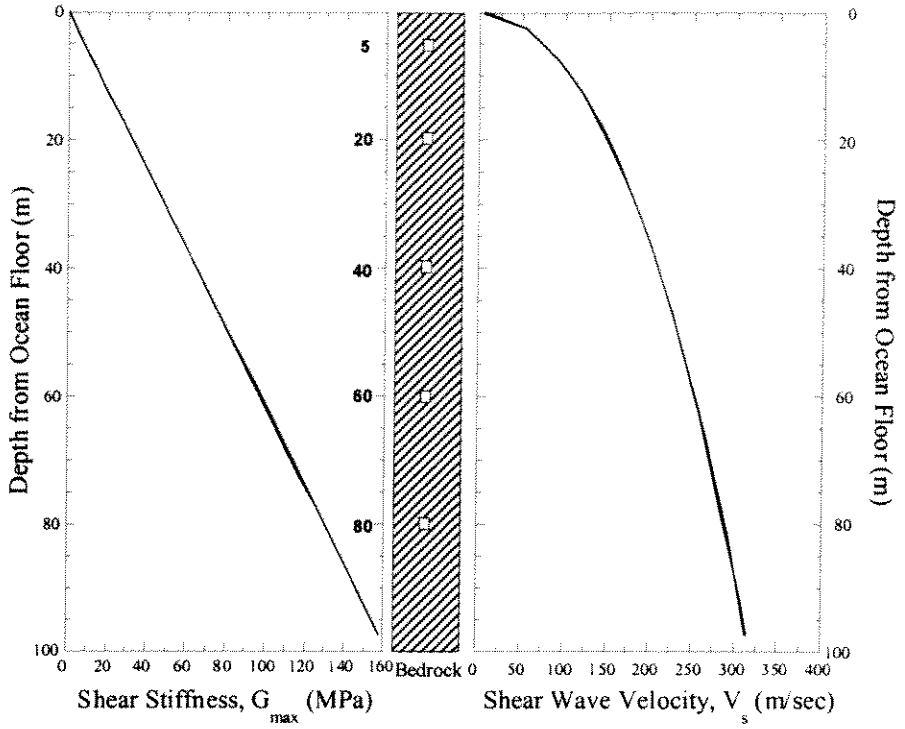

Fig A2.4 Shear modulus and shear wave velocity profiles considered for the example normally consolidated soil profile

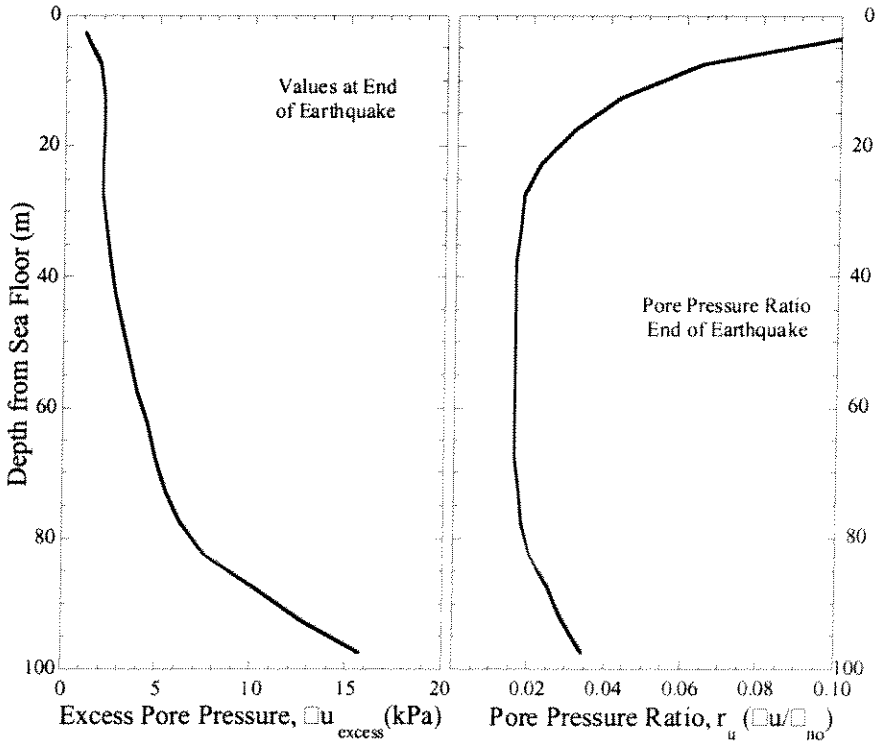

Figure A2.5 Generated excess pore pressures due to a strong earthquake event.

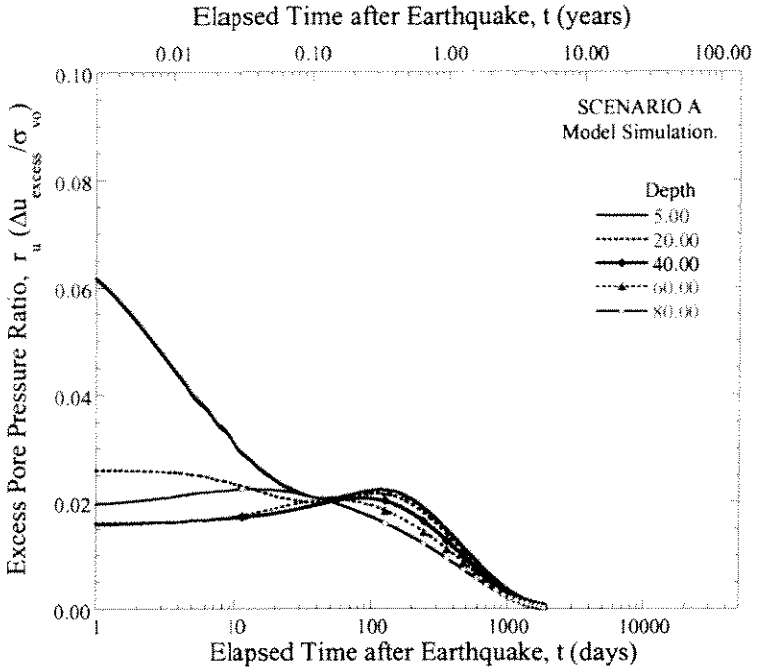

Figure A2.6 Dissipation of earthquake-generated excess pore pressures in a uniform soil profile.

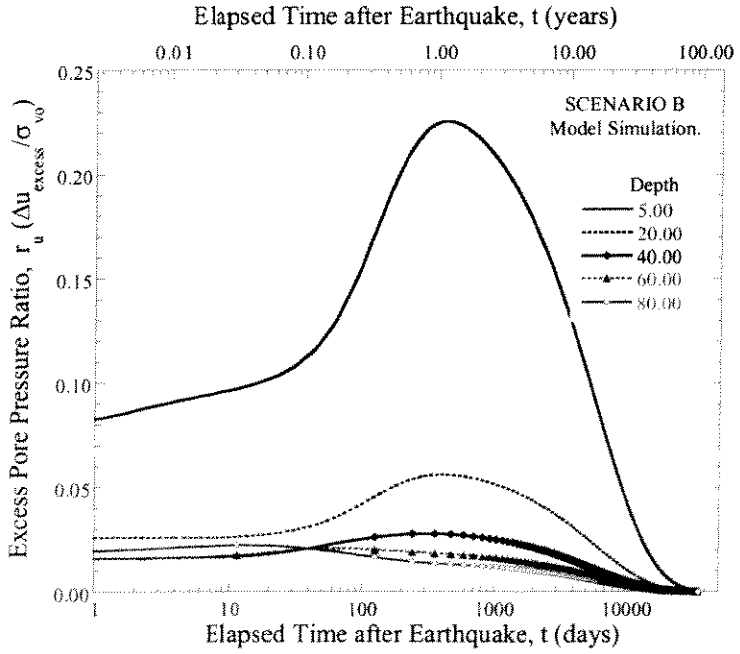

Figure A2.7 Dissipation of earthquake-generated excess pore pressures in a soil profile with a very low permeability layer at 5 m depth.

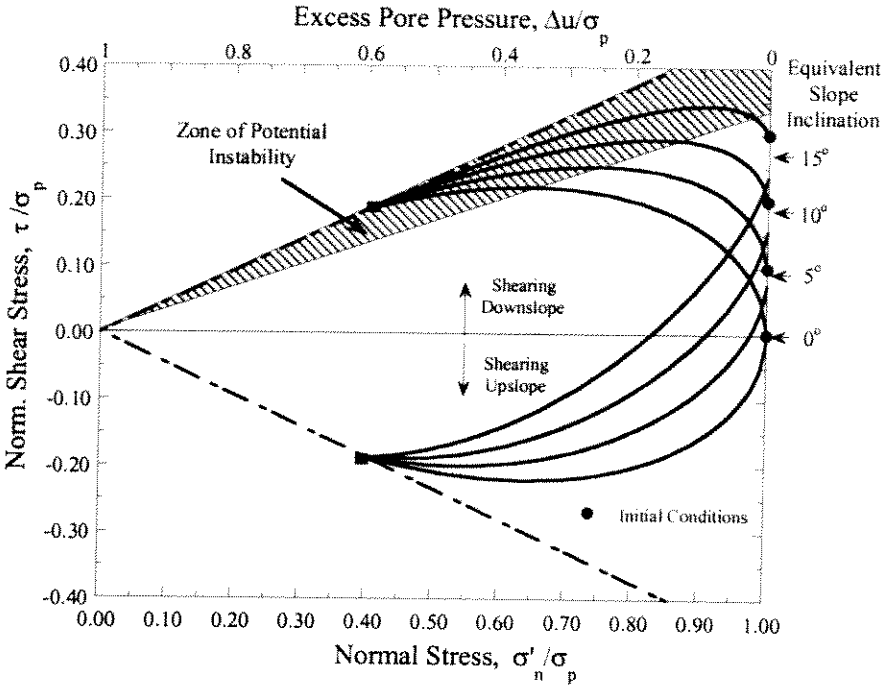

Figure A2.8 Effective stress paths for undrained monotonic loading of normally consolidated clay (Pestana, 2000).

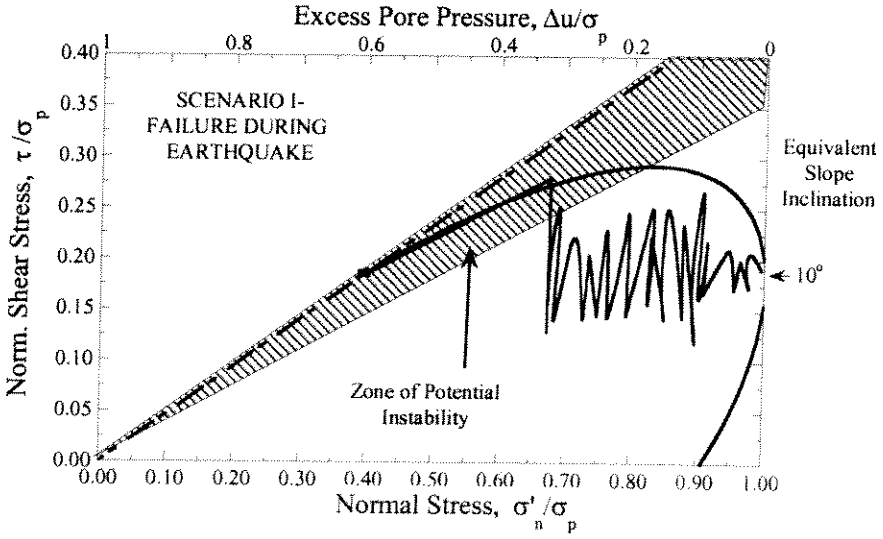

Figure A2.9 Effective stress path for a soil element on the critical slip surface when slope failure occurs during earthquake (Scenario 1).

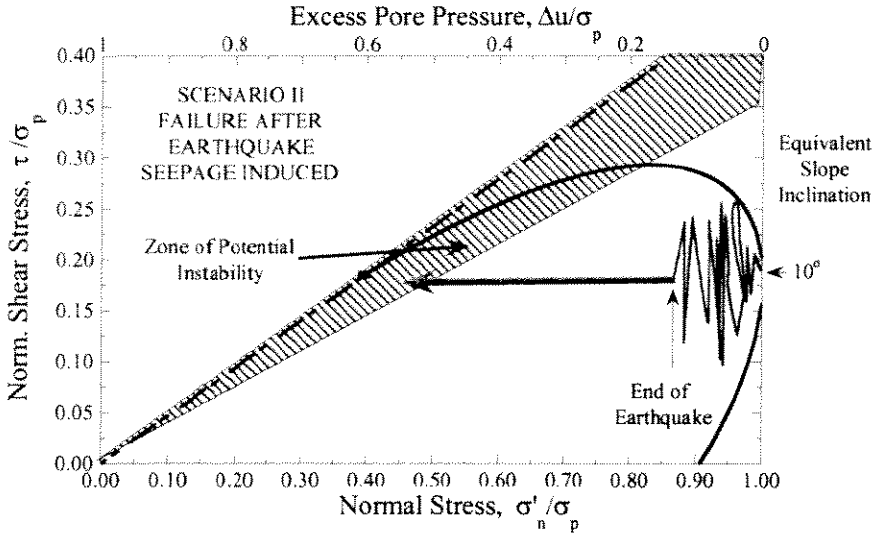

Figure A2.10 Effective stress path for a soil element on the critical slip surface when slope failure occurs after the earthquake due to seepage (Scenario 2).

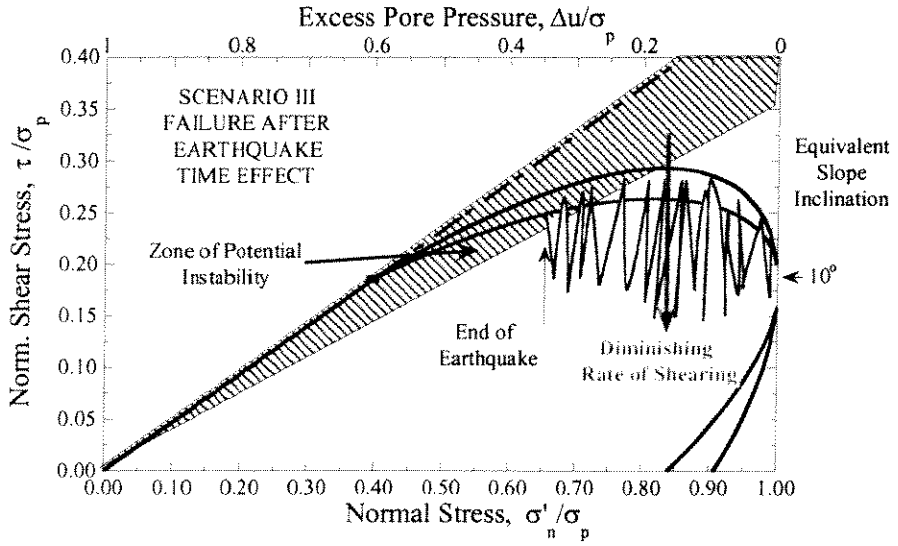

Figure A2.11 Effective stress path for a soil element on the critical slip surface when slope failure occurs after the earthquake due to creep (Scenario 3).

Other load effects

The vertical component of earthquake motion is often ignored in the evaluation of the seismic stability of sea floor. The reason is that in a dynamic stability evaluation of a submarine clay slope, where the soil response is essentially undrained during the earthquake loading, the earthquake-induced stresses normal to a potential failure surface are not important. Because of the lack of drainage during the earthquake, the changes in the normal stress are equal to the changes in the pore water pressure and the effective stress, which governs the soil behaviour, remains unchanged.

The above rationale may not be valid if there is free gas in the pore water. In this situation, the temporary, rapid pressure changes caused by the vertical component of motion may lead to expansion of the gas bubbles and cause the sediments to become unstable. As far as we know, this mechanism has not been looked into before and more research is needed to establish whether this is a viable phenomenon.

References

Kramer, S.L. (1996). Geotechnical earthquake engineering. Prentice-Hall International Series in Civil Engineering and Engineering Mechanics.

Nadim, F., B. Kalsnes, and A. Eide 1996. Analysis of submarine slope stability under seismic action. *Proc. 7th ISL*: 561-565. Rotterdam: Balkema.

Nadim, F., and B. Kalsnes (1997). Evaluation of clay strength for seismic slope stability analysis. Proc., XIV ICSMFE, Hamburg, Germany, Vol. 1, pp 377-379, 6-12 September.

Newmark, M.N. (1965). Effects of earthquakes on dams and embankments. Geotechnique, Vol. 15, No. 2, pp 139 - 160.

Norwegian Geotechnical Institute (1997). Earthquake hazard and submarine slides – Submarine slides: A literature survey. NGI report 963014-1, 14 February.

Norwegian Geotechnical Institute (1999). Earthquake hazard update and slope stability evaluation – Evaluation of slope stability and submarine slides. Report SP-29-NG-02R-00000-99 prepared for The Seabed Group. NGI report 982512-2, 30 July.

Pestana, J.M. (2000). New soil model for static and dynamic response of soft clays. (NGI report under preparation).

Pestana, J.M., and F. Nadim (2000). New version of AMPLE for seismic stability analysis of slopes. (NGI report under preparation).

Robertson, P.K., and C.E. Fear (1995). Liquefaction of sands and its evaluation. IS TOKYO '95, First International Conference on Earthquake Geotechnical Engineering, Keynote Lecture, November 1995.

Seed, H. B., I. M. Idriss, and I. Arango (1983). Evaluation of liquefaction potential using field performance data. Journal of Geotechnical Engineering, ASCE, Vol. 109, No. 3, March 1983.

Technical Committee for Earthquake Geotechnical Engineering, TC4, ISSMGE (1999). Manual for zonation of seismic geotechnical hazards (revised version). Published by the Japanese Geotechnical Society, Tokyo, Japan.

APPENDIX 3: CENTRIFUGE DEMONSTRATION TEST INFORMATION AND DATA

A3.1 Demonstration Test 1: Strong Box Instrumentation and Test Set Up

Strong Box and Instrumentation

Strongbox

The strongbox, or model testing container, has inside dimensions of 900 mm long by 300 mm wide and a depth of 420 mm. One side of the box consists of a plexi-window so that a cross section of the slide can be seen in order to measure the displacement of the slurry mixture. The strongbox has two drainage ports at the base along the longitudinal centerline. Plumbed into the drainage ports is a standpipe, open to atmospheric pressure, which dictates the maximum achievable water level within the model. The base of the soil container was covered with geotextile to prevent the two drain ports from clogging. Above this layer of geotextile is a 30 mm thick layer of drainage sand that is again covered with a layer of geotextile. The perimeter of the geotextile was sealed with utility tape to prevent flow of the silty clay slurry from entering and clogging the sand layer.

At the dead centre midpoint of the soil model a pore pressure induction nozzle was present at 115 mm above the sand layer. This nozzle was plumbed to an external valve.

A photograph of the strongbox after testing is included as Figure 8.5.

PPT

Pore water pressure was measured using 6 PPT's. Five of the PPT's were positioned within the slurry at various depths and locations. One PPT was positioned outside the slurry at the external valve for the pore pressure induction nozzle. Originally, 4 PPT's were placed in the slurry at points labeled, Head, Mid-Body, Toe, and Mid-Body Nozzle. After consolidation, 2 additional PPT's were added to the head of the slurry surface, labeled Head 1 and Head 2. The positions of the PPT's are shown in Figure 8.6

Additional Instrumentation

Additional apparatus was mounted to the strongbox with the intention of exerting additional stresses on the soil surface. These operations were intended to be conducted, after the slurry was completely consolidated.

To simulate due to sedimentation, a pan of loose sand was mounted to the top of the strongbox, above the head of the slope. The pan was tethered to a pulley system, that, when activated, could rotate the pan slightly to release sand onto the head of the slope.

A cone penetrometer was mounted in the centre of the strongbox.

Test Setup

The modelling soil was comprised of 50% Speswhite Fine China kaolin clay and 50% Sil-Co-Sil silt. A 5 HP Bowers clay mixer with a 200 litre capacity was used to reconstitute the material.

The material was mixed under vacuum at a water content of 70% and a mixing rate of 14 rpm for about 44 hours.

The silty clay slurry with a water content of 70%, was flowed into the model container and worked by hand to eliminate any entrapped air pockets. The slurry was placed to a nominal thickness of 286 mm. The container was then placed on the 4° incline where the level of the material was then trowelled by hand to maintain a level surface with respect to the base of the centrifuge platform.

A3.2 Demonstration Test 2: Strong Box Instrumentation and Test Set Up

Strongbox and Instrumentation

Strongbox

The strongbox, or model testing container, has an inside diameter of 900 mm long by 300 mm wide and a depth of 420 mm. One side of the box consists of a plexi-window so that a cross section of the slide can be seen in order to measure the displacement of the slurry mixture. The strongbox has two drainage ports at the base along the longitudinal centerline. Plumbed into the drainage ports is a standpipe, open to atmospheric pressure, which dictates the maximum achievable water level within the model. The base of the soil container was covered with geotextile to prevent the two drain ports from clogging. Above this layer of geotextile is a 67.5 mm thick layer of drainage sand that is again covered with a layer of geotextile. The perimeter of the geotextile was sealed with utility tape to prevent flow of the silty clay slurry from entering and clogging the sand layer.

At the dead centre midpoint of the soil model a pore pressure induction nozzle was present at 115 mm above the sand layer. This nozzle was plumbed to an external valve.

A photograph of the strongbox after testing is included as Figure A3.1.

PPT

Pore water pressure was measured using 6 PPT's. Five of the PPT's were positioned within the slurry at various depths and locations. One PPT was positioned outside the slurry at the external valve for the pore pressure induction nozzle. During phase 1 consolidation, 3 PPT's were placed in the slurry at points labeled, Sand Drain, Toe, and PWP Injector. After phase 1 consolidation, 4 additional PPT's were added to the slurry surface, labeled Head, Head 1, Head 2, and Mid Body. The positions of the PPT's are shown in Figure A3.2.

Additional Instrumentation

Additional apparatus was mounted to the strongbox with the intention of exerting additional stresses on the soil surface. These operations were intended to be conducted, after the slurry was completely consolidated.

To simulate due to sedimentation, a pan of loose sand was mounted to the top of the strongbox, above the head of the slope. The pan was tethered to a pulley system, that, when activated, could rotate the pan slightly to release sand onto the head of the slope.

A cone penetrometer was mounted in the centre of the strongbox.

Test Setup

The modelling soil was comprised of 50% Speswhite Fine China kaolin clay and 50% Sil-Co-Sil silt. A 5 HP Bowers clay mixer with a 200 litre capacity was used to reconstitute the material. The material was mixed under vacuum at a water content of 70% and a mixing rate of 14 rpm for about 44 hours.

The silty clay slurry with a water content of 70%, was flowed into the model container and worked by hand to eliminate any entrapped air pockets. The slurry was placed to a nominal thickness of 235 mm. The container was then placed on the 4° incline where the level of the material was then trowelled by hand to maintain a level surface with respect to the base of the centrifuge platform.

A3.3 PODS Centrifuge Demonstration History

Demonstration 1

Date: January 22 - 23, 2001
Centrifuge Operator: Don Cameron
Centrifuge User: Richard Hanke

Slope Model:

The base of the strong box was covered in geotextile. A layer of sand, 30 mm thick, was then placed on top of this matting and an additional layer of geotextile was placed over the sand. The slurry mixture consisted of 50% Speswhite Fine China kaolin clay and 50% Sil-Co-Sil silt. The slurry was poured into the strongbox to a thickness of 285 mm. The strongbox was placed on a 4° wedge.

Demonstration Summary:

The test pacakge underwent phase 1 consolidation for 4 1/2 hours on a 4° slope at 80g. Once the package was removed from the centrifuge, the wedge beneath the box was rotated 180° and the specimen was mounted back inside the centrifuge. Once the test box reached 35g, the slope failed.

Viewing Results:

Spaghetti strands were placed vertically in the slurry next to the plexi-window.

Demonstration 2

Date: March 8 – 9, 2001
Centrifuge Operator: Derry Nicholl
Centrifuge User: Richard Hanke

Slope Model:

The slope was modeled similarly to Demonstration 1, with 2 exceptions. The composition of the slurry was the same as in demonstration 1. The sand layer at the bottom of the strongbox was increased to 67.5 mm in thickness. The slurry thickness was reduced to 235 mm. The strongbox was again placed on the 4° wedge.

Demonstration Summary:

For this demonstration, phase 1 consolidation was extended to 8 hours on a 4° slope at 80g. Once the package was removed from the centrifuge, the wedge beneath the box was rotated 180° and the specimen was mounted back inside the centrifuge. Phase 2 consolidation proceeded by increasing the g force on the specimen in half-hour intervals from 10, 20, 40, 60, 70, and 80g. At

60g, the slope failed. The demonstration continued to test speed; however, no visible changes could be seen to the slide surface when the pore water pressure was raised or sediment loading was applied to the head of the slope.

Viewing Results:

Darker spaghetti was placed vertically in the slurry next to the plexi-window. Small pieces of colored pasta were also placed in a grid formation on top of the slurry. The darker spaghetti strands were more visible than those used in demonstration 1, however the pieces of pasta could not be seen after the slide had failed.

Table A3.1: Water Content Determination, Test1

Boring No.	1	2	3	4
Boring Depth	11.7	87.3	103.4	156.4
Container no. (cup)	1	2	3	4
Mass of cup + wet soil	286.5	424	465.3	341.1
Mass of cup + dry soil	179.2	276.3	303.8	242.1
Mass of cup	3.6	3.6	3.6	3.6
Mass of dry soil, M_s	175.6	272.7	300.2	238.5
Mass of water, M_w	107.3	147.7	161.5	99
Water Content, w %	61.1	54.2	53.8	41.5

Boring No.	5	6	7	8
Boring Depth	102.6	197.2	159.8	211.3
Container no. (cup)	5	6	7	8
Mass of cup + wet soil	328.3	213.8	235.3	193.6
Mass of cup + dry soil	219.5	154.6	169.1	142.6
Mass of cup	3.6	3.7	3.4	4.2
Mass of dry soil, M_s	215.9	150.9	165.7	138.4
Mass of water, M_w	108.8	59.2	66.2	51
Water Content, w %	50.4	39.2	40	36.9

Table A3.2: Pore Water Pressure Depths, Test 1

Location	Depth Below Surface (mm.)
Sand	**?**
Head	171.9
Head 1	157.8
Head 2	97.8
Mid Body	90.1
Toe	10.2

Table A3.3: Vane Test Position and Results, Test 1

Test Site Number	Depth below surface (mm.)	Result
1	103.8	0.5
5	103.8	1
2	148.2	1
3	189.4	3.25
4	189.4	1.75
6	195	3.25

Table A3.4: Water Content ... Distribution, Test 2

Site Number	Depth (mm)	Distance from Head (mm)	Moisture Content (w%)
1	10	755	45.3
2	10	450	42.5
3	10	150	43.3
4	90	770	39.1
5	90	400	38.5
6	95	135	38.4
7	175	770	36.1
8	175	400	35.5
9	180	135	35.3

Note: 7, 8, and 9 were at the ... textile surface

Table A3.5: Pore Water Pressure Locations, Test 2

Location	PPT Number	Depth (mm)	Distance from Head (mm)
Head	9494	32	75
Head 1	8058	49	50
Head 2	8062	48	45
Mid Body	9496	70	500
Toe	9099	145	810

Table A3.6: Vane Test Results

		Depth = 60mm	Depth = 120mm	Remolded (depth=60mm)
Test Site No.	Distance from Head (mm)	Result (kPa)	Result (kPa)	Result (kPa.)
1	760	3.2	5.8	4
2	415	2.8	6.3	4
3	125	4	8.2	3

Note: Vane Tests conducted ...

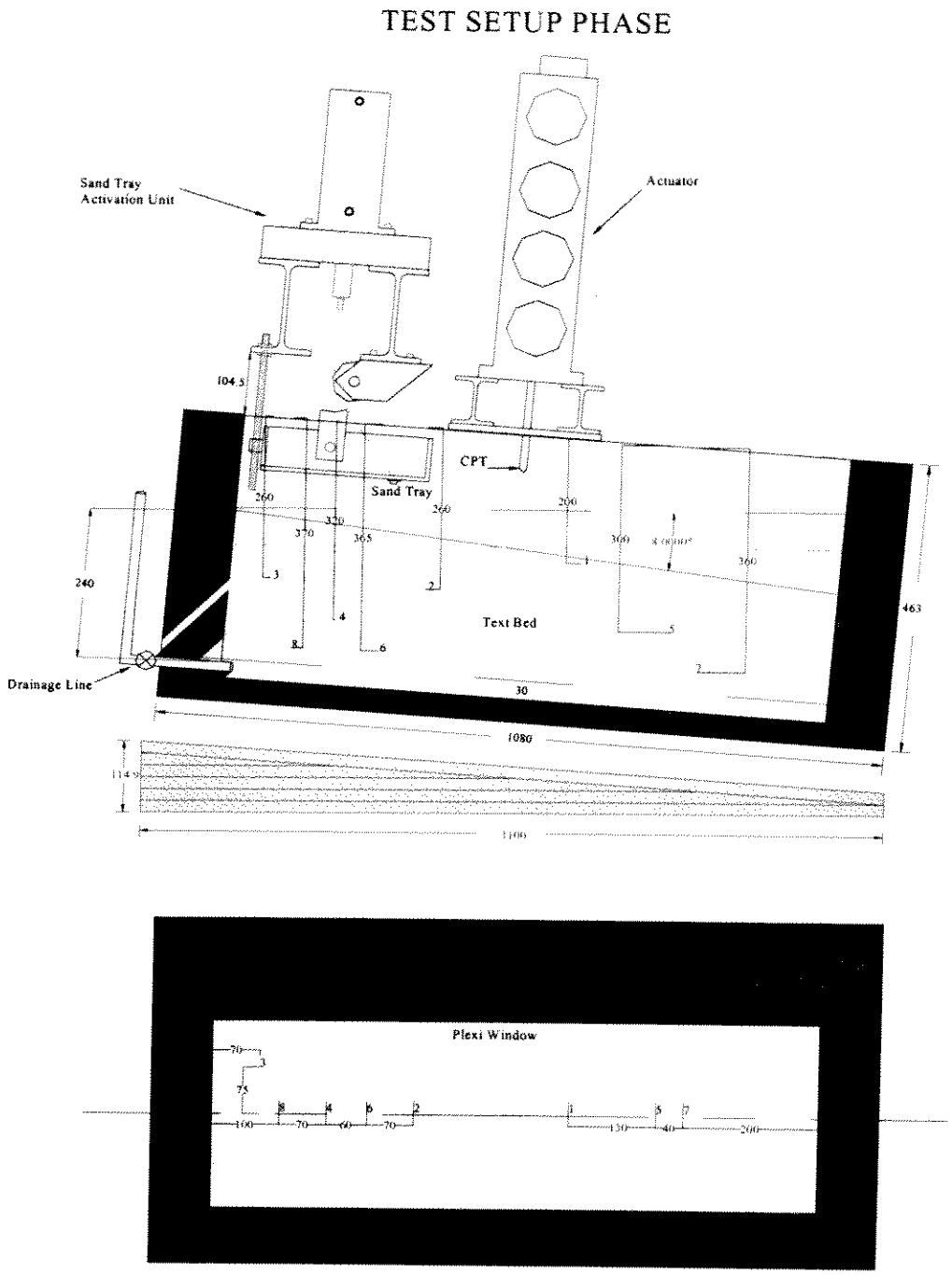

Figure A3.1: Moisture Content Locations, Test 1

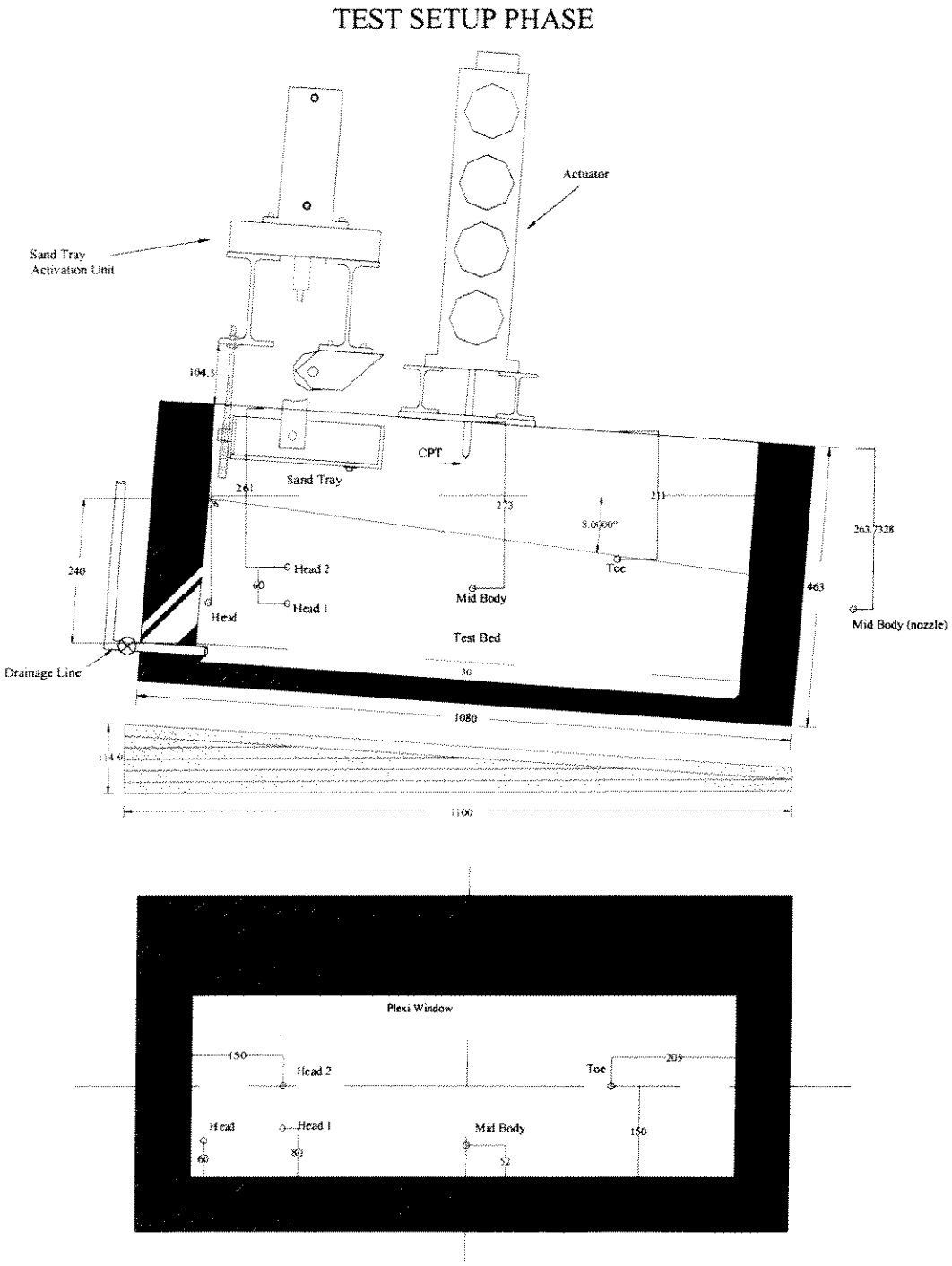

Figure A3.2: Vane Test Locations, Test 1

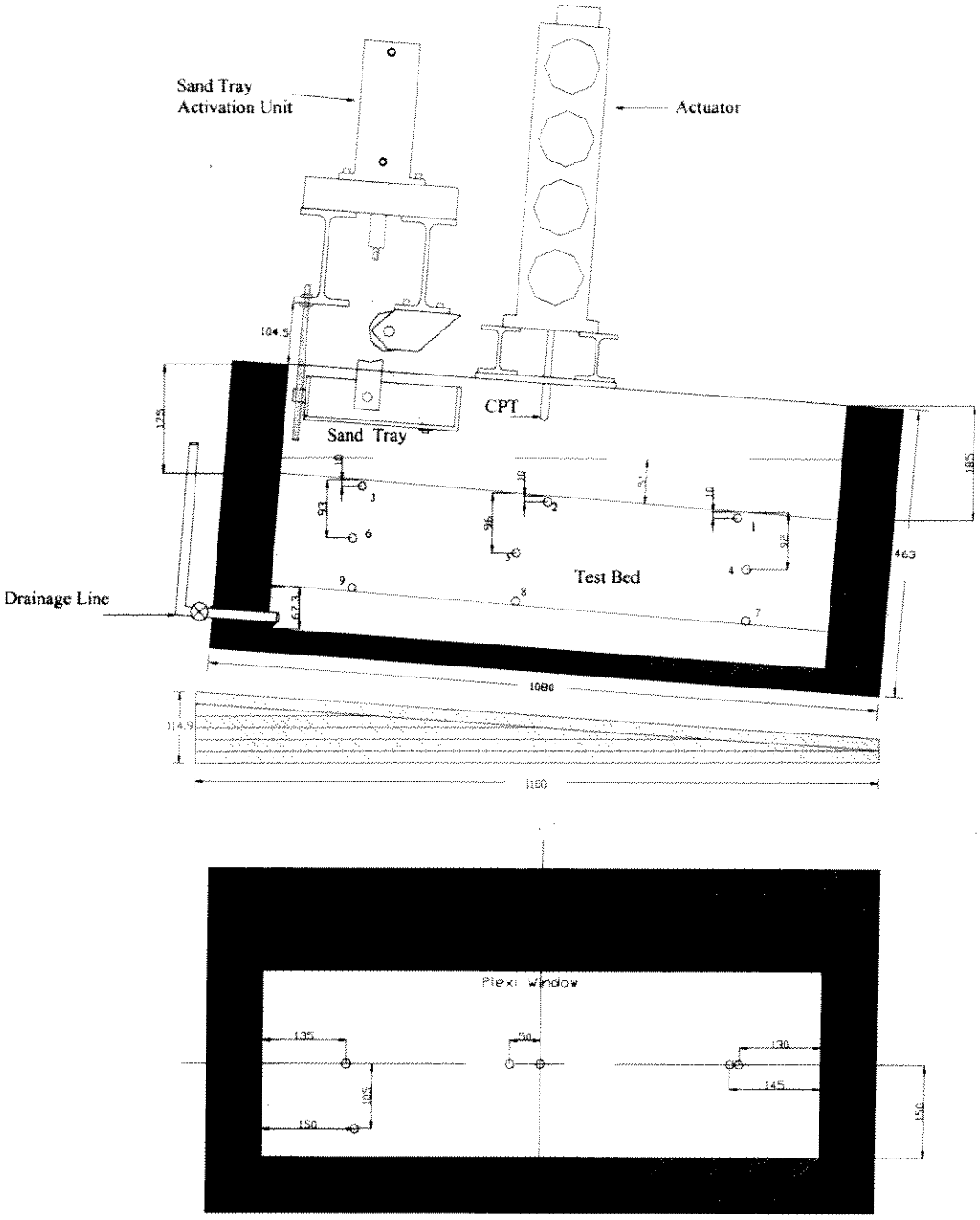

Figure A3.3: Moisture Content Locations, Test 2

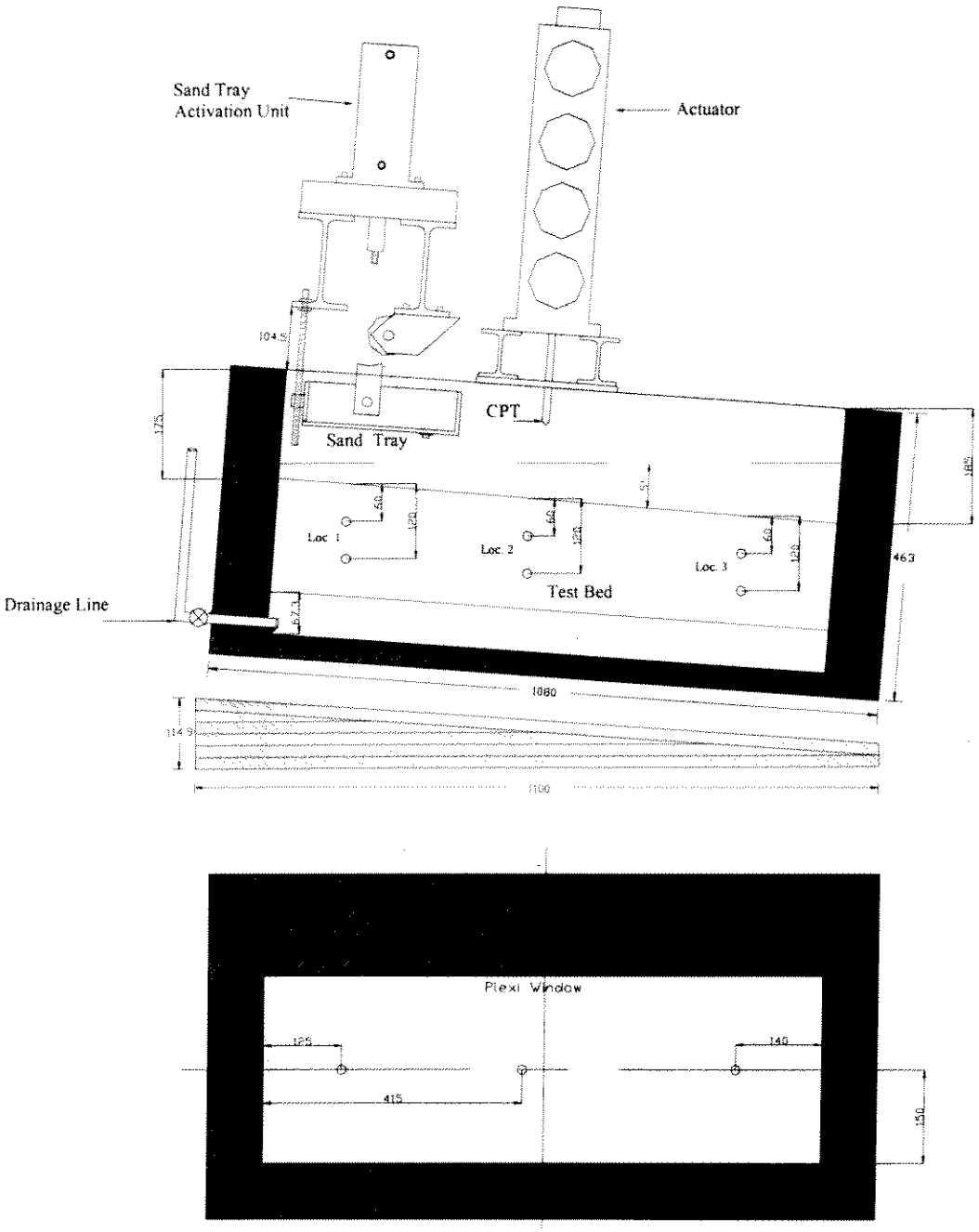

Figure A3.4: Vane Test Positions, Test 2

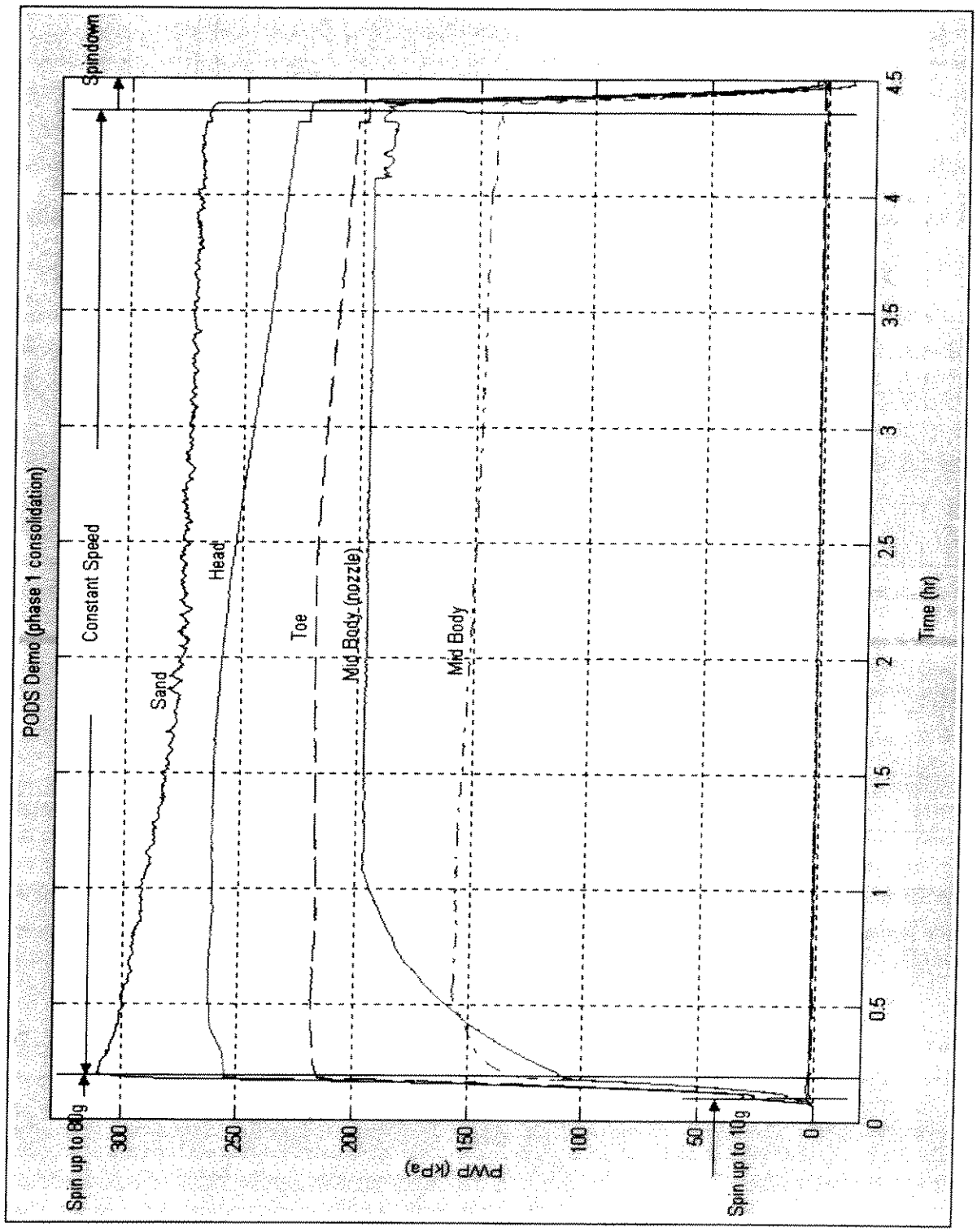

Figure A3.5 Phase 1 Consolidation PPT Measurements, Test 1

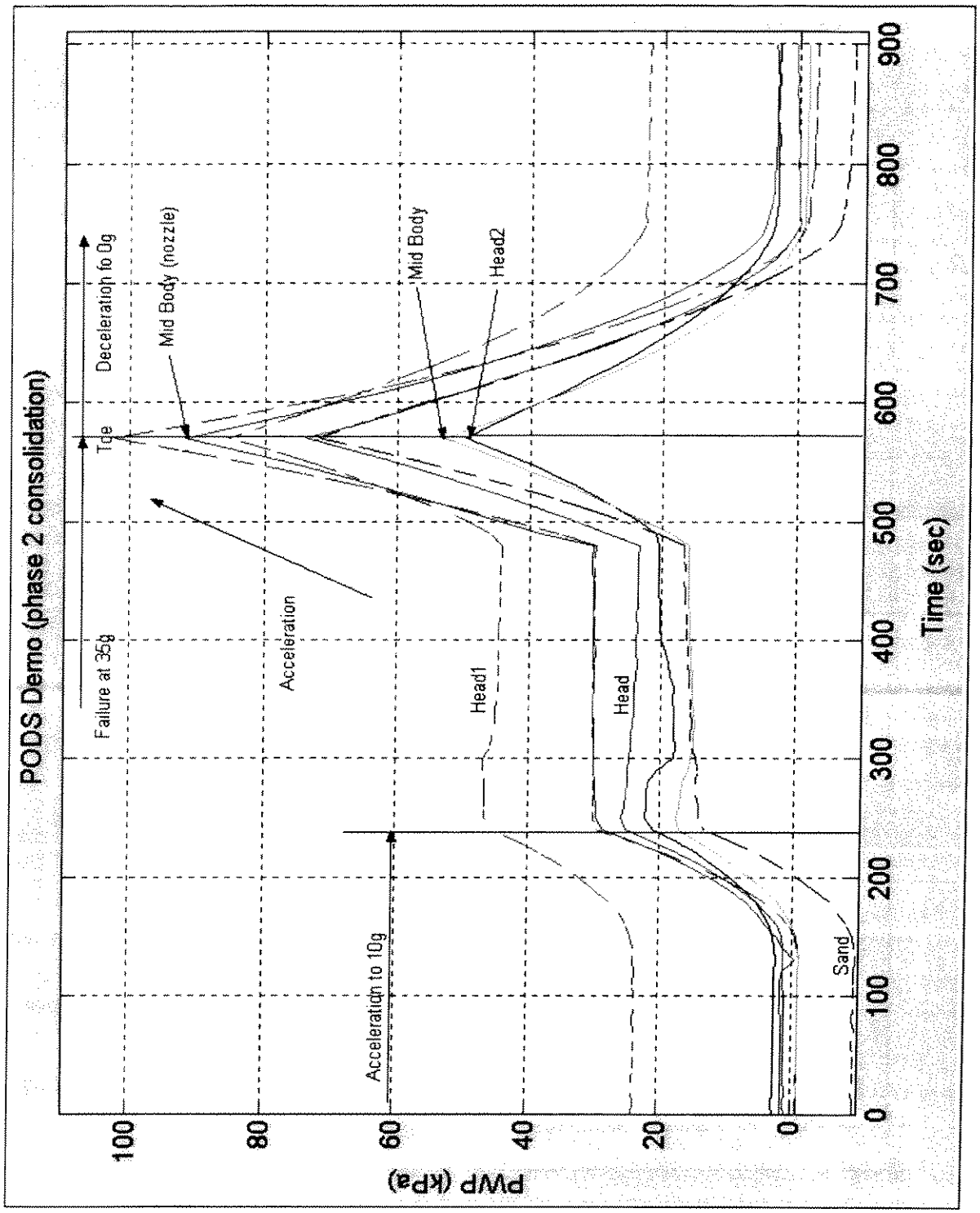

Figure A3.6 Phase 2 Consolidation PPT Measurements, Test 1

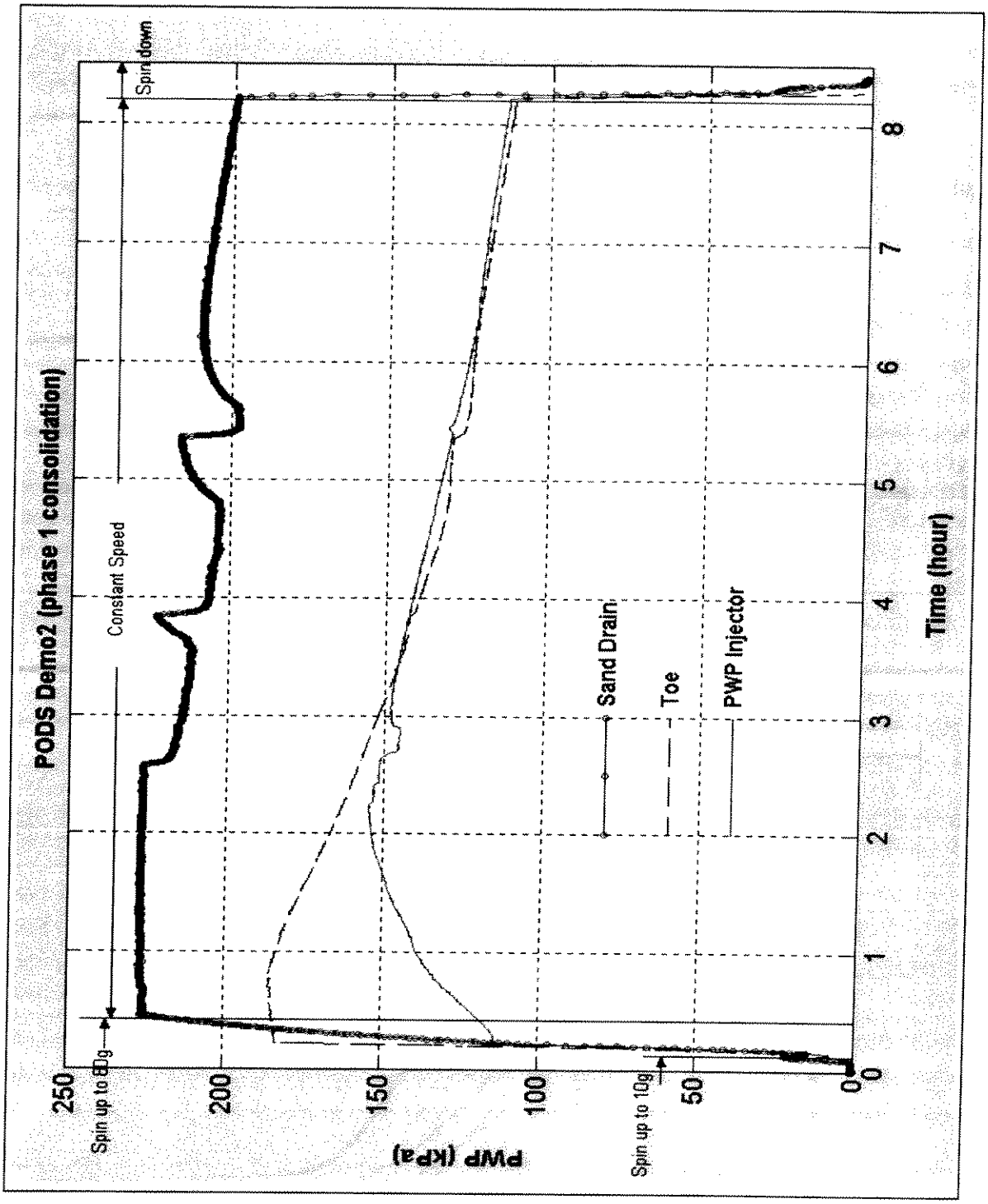

Figure A3.7 Phase 1 Consolidation PPT Measurements, Test 2

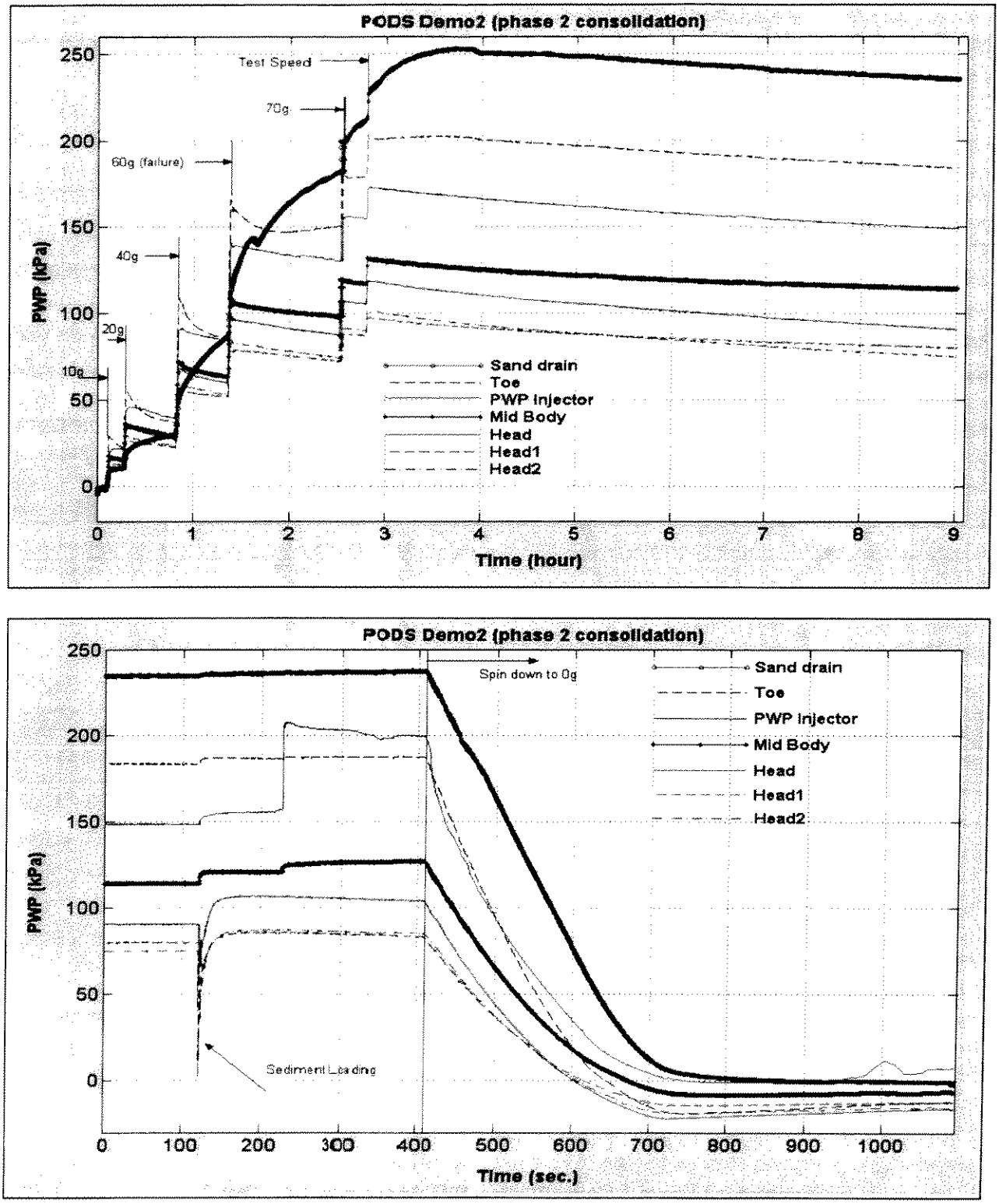

Figure A3.8 Phase 2 Consolidation PPT Measurements, Test 2

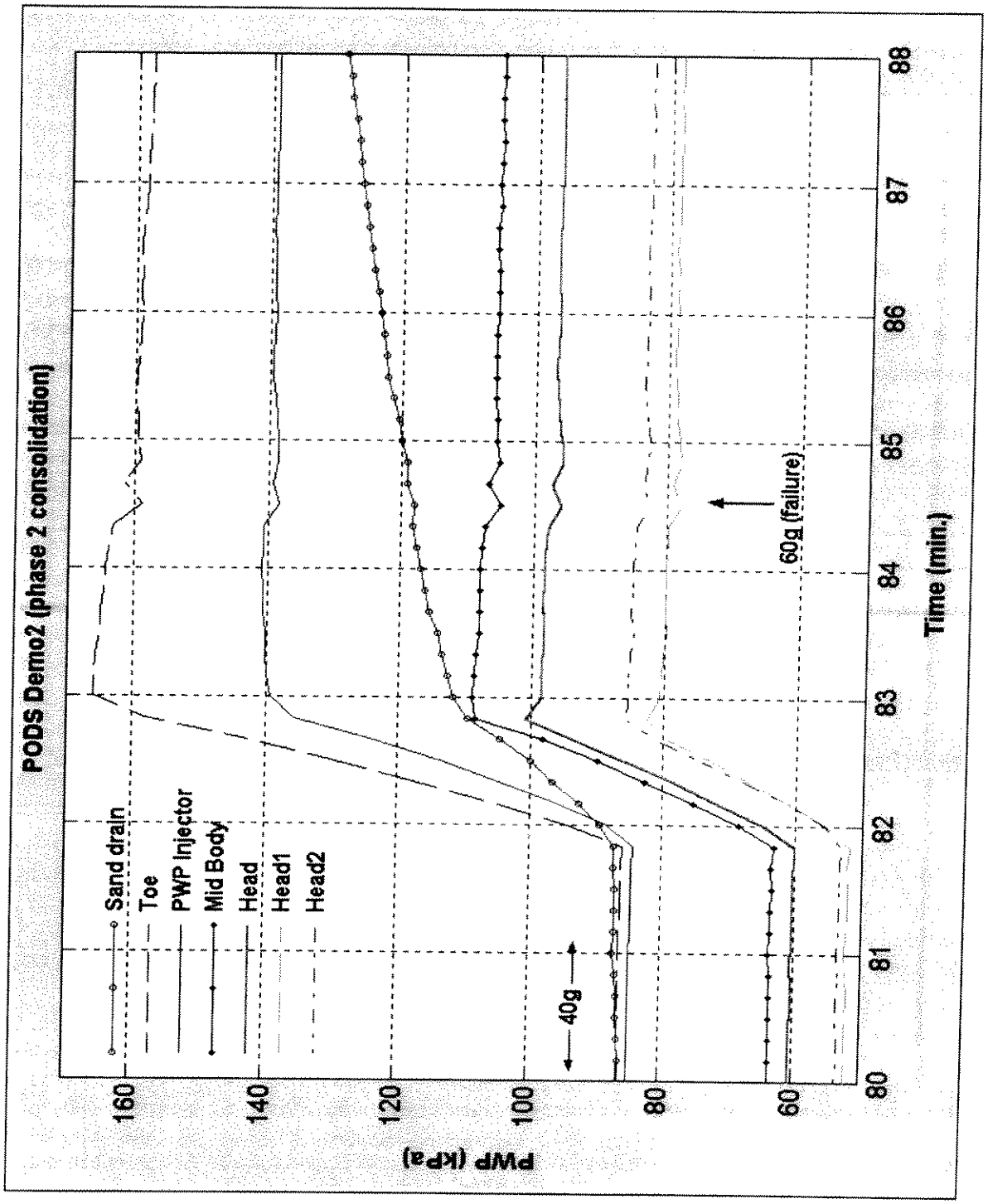

Figure A3.9 PPT Measurements at Failure at 60g, Test 2

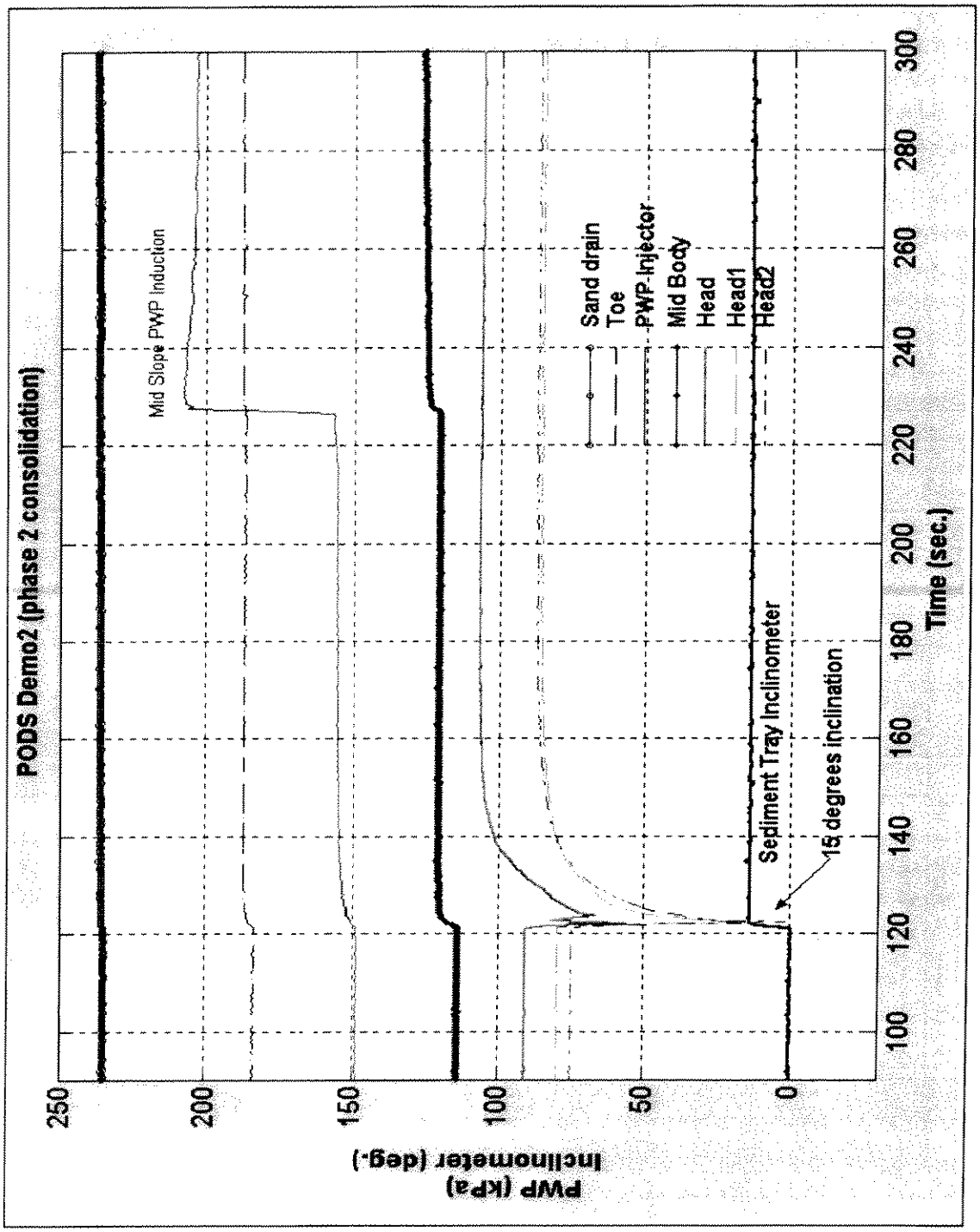

Figure A3.10 PPT Measurements During Slide Triggering, Test 2

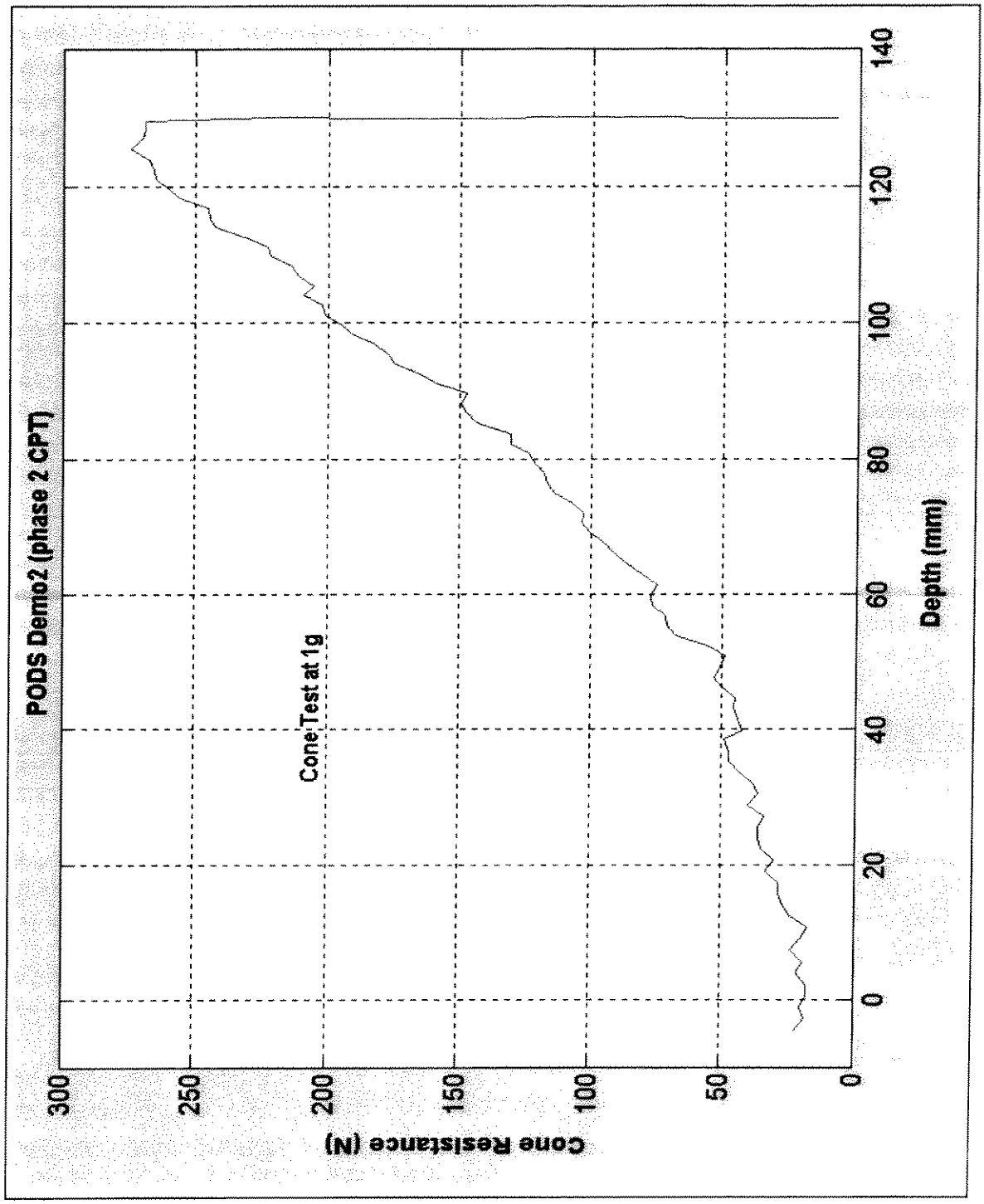

Figure A3.11 Cone Penetrometer Test, Test 2